

Anh Tran

**HIGHLY STABLE AND EFFICIENT LEAD-BASED  
PEROVSKITE SOLAR CELL WITH TIN-OXIDE  
ELECTRON TRANSPORT LAYER**

Bachelor of Science Thesis  
Faculty of Engineering and Natural Sciences  
Examiners: Associate Prof. Paola Vivo  
Doctoral Researcher Noora Lamminen  
October 2023

## ABSTRACT

Anh Tran: Highly stable and efficient lead-based perovskite solar cell with tin-oxide electron transport layer  
Bachelor of Science Thesis  
Tampere University  
Sciences and Engineering  
October 2023

---

Fossil fuels still hold a predominant position in global energy consumption. However, they have caused various environmental and societal problems. The world's energy demand has been increasing tremendously over the years, which results in an urgent need to utilize more alternative energy sources. In the quest for sustainable and renewable energy sources, solar energy is known to be a promising solution to address the growing global energy demand and environmental concerns. Photovoltaics (PV) refers to applications harvesting solar energy and generating electricity. Over the past few decades, the capacity and technologies of PV have grown noticeably with various materials and architectures being studied to enhance efficiency, stability and cost-effectiveness. Among generations of PV cells, halide perovskite solar cells (PSCs) in the third generation show remarkable properties that set them apart from conventional photovoltaic technology. Even though perovskite solar cells are still a new PV technology compared to other solar cells, it has gained interest from scientists and researchers worldwide. Its power conversion efficiency (PCE) has increased exponentially over a short period of time, from 3.8 % in 2009 to 26.1 % in 2023. Despite many advantages, a well-known obstacle preventing perovskite solar cells from viable commercialization is their instability because of many degradation pathways.

The main focus of this thesis is the effect of the nanoparticle tin-oxide-based electron transport material on the performance of lead-halide perovskite solar cells. Electron transport materials (ETMs) in solar cells facilitate the movement of electrons generated by absorbed sunlight towards the electrical contacts, enabling the conversion of solar energy into electricity. By using a suitable ETM in a solar cell, electron mobility within the cell can be improved. Titanium-oxide-based electron transport material, one of the most common ETMs for lead-halide perovskite solar cells, is chosen as a reference to compare with the tin-oxide-based ETM. Tin-oxide ( $\text{SnO}_2$ ) enhances charge mobility due to a deeper conduction band than titanium-oxide ( $\text{TiO}_2$ ). The manufacturing process of the  $\text{SnO}_2$ -based perovskite solar cells does not require high temperatures - a common disadvantage in the production of  $\text{TiO}_2$ -based solar cells. In this thesis, two different concentrations of nanoparticle stock solution were assumed and tested to choose the concentration resulting in more efficient perovskite solar cells. The nanoparticle stock solution was diluted with ultra-clean  $\text{H}_2\text{O}$  to a concentration of 2.67 % from the stock solution when assuming concentrations of 15 % and 20 %. Two types of substrate FTO and ITO were tested to observe which one is more suitable for nanoparticle  $\text{SnO}_2$ -based perovskite solar cells. PV characteristics and quantum efficiency measurements were assessed one day after solar cell fabrication had been completed. The cells with the best performance were chosen as samples for testing stability. Maximum power point tracking (MPPT) was conducted in an inert atmosphere.

The highest power conversion efficiency of 14.6 % was achieved on FTO substrates with  $\text{SnO}_2$  2.67 % concentration. The average PCE was 11.30 %. The fill factor (FF) values could reach 70.4 % with the average FF being 56.8 %. The external quantum efficiency (EQE) of  $\text{SnO}_2$ -based PSC was approximately 80 %. The  $\text{SnO}_2$ -based devices retained approximately 60 % of their initial

PCE after 100 hours, which indicates their high stability. Despite the lower results compared to TiO<sub>2</sub>-based devices, SnO<sub>2</sub>-based devices showed promising performance in PCE and stability. Further research could focus on SnO<sub>2</sub> recipes and their effect on the performance and stability of perovskite solar cells.

Keywords: Halide perovskite solar cell, electron transport material, SnO<sub>2</sub>-based solar cell, stability

The originality of this thesis has been checked using the Turnitin OriginalityCheck service.

## **PREFACE**

This thesis was done in the Hybrid Solar Cells (HSC) team of the Chemistry and Advanced Materials group at Tampere University and was supervised by Associate Professor Paola Vivo and Doctoral Researcher Noora Lamminen. I would like to thank them for guiding and helping me to complete my thesis on an interesting novel topic. I appreciate their feedbacks that helped me improve this thesis. This thesis would not have been able to exist without their invaluable help. I also appreciate meaningful support from my girlfriend and family while writing this thesis.

Tampere, 18th October 2023

Anh Tran

## CONTENTS

|       |   |    |
|-------|---|----|
| 1.    | Introduction  | 1  |
| 2.    | Theoretical background                                    | 3  |
| 2.1   | Basic principle of PV cells                               | 3  |
| 2.1.1 | Charge separation and recombination                       | 5  |
| 2.1.2 | Characteristics and parameters                            | 6  |
| 2.1.3 | Stability of devices                                      | 8  |
| 2.2   | Lead halide perovskite solar cells                        | 9  |
| 2.2.1 | Perovskite and perovskite solar cell (PSC)                | 9  |
| 2.2.2 | Mesoporous and planar structures in perovskite solar cell | 12 |
| 2.2.3 | Electron transport layer                                  | 13 |
| 3.    | Materials and methods                                     | 16 |
| 3.1   | Tin-based electron transport material                     | 16 |
| 3.2   | Solar cell manufacturing                                  | 17 |
| 3.2.1 | Substrate and electrodes                                  | 17 |
| 3.2.2 | Electron transport layer                                  | 19 |
| 3.2.3 | Perovskite layer  | 20 |
| 3.2.4 | Hole transport layer                                      | 20 |
| 3.2.5 | UV Ozone (UVO) treatment                                  | 21 |
| 3.3   | Efficiency and stability measurement                      | 21 |
| 3.3.1 | J-V measurement   | 21 |
| 3.3.2 | Quantum efficiency measurement                            | 22 |
| 3.3.3 | Stability measurement                                     | 23 |
| 4.    | Results and discussion                                    | 24 |
| 4.1   | Solar cell performance                                    | 24 |
| 4.2   | Solar cell stability in MPPT measurement                  | 32 |
| 5.    | Conclusion  | 34 |
|       | References  | 36 |

## LIST OF SYMBOLS AND ABBREVIATIONS

|                    |  |
|--------------------|--|
| $J$                | Current  |
| $J_{sc}$           | Short-circuit current density  |
| $P_{max}$          | Maximum generated power  |
| $V$                | Voltage  |
| $V_{oc}$           | Open-circuit voltage   |
| c-TiO <sub>2</sub> | Compacttitanium dioxide  |
| 2G                 | Second Generation  |
| 3G                 | Third Generation   |
| CIGS               | Copper-Indium-Gallium-Selenide   |
| CsMAFA             | Cs <sub>0.05</sub> (MA <sub>0.17</sub> FA <sub>0.83</sub> ) <sub>0.95</sub> Pb(I <sub>0.83</sub> Br <sub>0.17</sub> ) <sub>3</sub> |
| DMF                | N,N-dimethylformamide  |
| DMSO               | Dimethyl sulfoxide   |
| EQE                | External quantum efficiency  |
| ETL                | Electron transport layer   |
| ETM                | Electron transport material  |
| FF                 | Fill factor  |
| FK209              | Tris(2-(1H-pyrazol-1-yl)-4-tert-butylpyridine)cobalt(III)-tris[bis(trifluoromethylsulfonyl)imide]                                  |
| FTO                | Fluorine-doped tin oxide   |
| HTL                | Hole transport layer   |
| IQE                | Internal quantum efficiency  |
| ISOS               | International Summit on Organic photovoltaic Stability standard  |
| ITO                | Indium-doped tin oxide   |
| Li-TFSI            | Bis(trifluoromethane)sulfonimide lithium salt  |
| m-TiO <sub>2</sub> | Mesoporous titanium dioxide  |
| MPPT               | Maximum power tracking point   |
| OECD               | Organization for Economic Co-operation and Development   |

|              |   |
|--------------|---|
| PCE          | Power conversion efficiency   |
| PSC          | Perovskite solar cell   |
| QE           | Quantum efficiency  |
| spiro-OMeTAD | 2,2',7,7'-Tetrakis[N,N-di(4-methoxyphenyl)amino]-9,9'-spirobifluorene |
| STC          | Standard Test Conditions  |
| tBP          | 4-tert-butylpyridine  |
| UVO          | Ultraviolet-ozone   |

## 1. INTRODUCTION

Utilizing renewable energy benefits societal development and environmental security, but fossil fuels are still indispensable to the global energy supply. [1] Massive reliance on fossil fuels and thermal energy sources has caused various environmental problems such as emissions of greenhouse gases and climate change. [2] It can also affect economic growth by enhancing income inequality. [3] Besides, there is a negative correlation between societal development and fossil fuel consumption. [4] Despite the limited non-renewable energy resources, the world's energy demand has been increasing over the years. The world's energy consumption increased from 12.62 Gtoe to 14.21 Gtoe in 10 years, raising interest in exploiting more alternative energy sources to solve the growing demand problem. [1] Replacing fossil fuel and thermal energy sources with renewable energy is a sustainable solution with many advantages. The growth of renewable energy consumption has driven the social equality status [5] and improved environmental quality [6]. Renewable energy also contributes to the sustainable development of countries and mitigates the effects of climate change. Over 10 years, the consumption of renewable energy has increased tremendously, by a factor of one in European countries, by two times in OECD countries, by three times in the world in total, and by approximately five times in non-OECD countries. [1]

In the quest for sustainable and renewable energy sources, photovoltaics (PV) have emerged as a promising solution to address the ever-growing global energy demand and environmental concerns. As the sun is a virtually limitless energy source, the demand for solar energy has exploded. The world's capacity of PV has increased 842 % over the last 10 years. [1] Over the past few decades, significant strides have been made in solar cell technology, with various materials and architectures being explored to enhance efficiency, stability, and cost-effectiveness. Solar cells or PV devices can be classified into three main generations. Starting from the silicon-based solar cells, which laid the foundation for modern solar technology, subsequent generations have emerged to overcome limitations and improve performance. Second-generation (2G) solar cells were conceived with a primary focus on cost-effectiveness, utilizing materials such as amorphous silicon and copper indium gallium selenide (CIGS). [7] Despite their lower production expenses, these 2G solar cells exhibited comparatively inferior performance when juxtaposed with their first-generation counterparts. This performance gap spurred the evolution of third-

generation (3G) technologies [8]. In recent times, there has been a discernible upsurge in the exploration and advancement of 3rd generation (3G) solar cell technologies. This spectrum encompasses a range of technologies, such as copper/zinc/tin sulfide, dye-sensitized, polymer, quantum dot, organic, and perovskite-based solar cells (PSCs). [7] Among these, perovskite solar cells have garnered immense attention as a revolutionary contender. This technology is promising to redefine the landscape of solar energy conversion.

Perovskite solar cells (PSC) exhibit remarkable properties that set them apart from conventional photovoltaic materials. The first PSCs were reported only in 2009. PSCs quickly gained interest from scientists, researchers, and many institutes worldwide because they possess a unique crystalline structure, which offers a versatile platform for achieving efficient light absorption and charge carrier generation. Over the years, recorded power conversion efficiency (PCE) has increased notably from 3.8 % to 26.1 % in 2023. [7] PSCs have many advantages and potential for commercialization. However, a well-known obstacle preventing PSCs from viable commercialization is their inherent instability. There are various factors affecting the degradation of PSCs. [9] The main focus of this thesis is the effect of the tin-oxide-based electron transport material on the performance of lead-based perovskite solar cells. The samples were assessed during the first week after fabrication and measured again after 7-14 days. The stability of the devices was also studied by measuring them under constant illumination under specific conditions for over 100 hours using maximum power point tracking (MPPT). Chapter 2 will provide some necessary theoretical background on photovoltaic devices and lead-halide perovskite solar cells. In Chapter 3, the fabrication process, methods, and materials are discussed, followed by a description of the testing and characterization of solar cells. Finally, Chapter 4 focuses on analyzing and discussing the collected data to make conclusions about the performance of the devices. This thesis aims to show the correlation between the tin-oxide-based electron transport layer and the enhanced overall performance of solar cells.

## 2. THEORETICAL BACKGROUND

This chapter will explain the fundamental mechanism of photovoltaic devices, followed by introducing characteristics and parameters that represent solar cell performance. Next, the instability factors of perovskite solar cells (PSCs) will be discussed. Finally, the perovskite solar cell structure and the effect of the electron transport layer on the solar cell performance will be discussed.

### 2.1 Basic principle of PV cells

Photovoltaic (PV) devices, commonly known as solar cells, are optoelectronic devices that convert sunlight directly into electricity through the photovoltaic effect. The photovoltaic effect, first discovered by E. Becquerel in 1839, involves the generation of electric current or voltage when certain materials are exposed to light. [10]

Semiconductor materials play a crucial role in the process of the photovoltaic effect. [10] A semiconductor is a material falling in the continuum between conductor and insulator. When substances are formed, they consist of many energy bands - different states that the electrons can occupy. [11] The electrons are filled in energy bands from the lowest unoccupied energy band following the Pauli exclusion principle. [11] [12] The energy band gap is the difference between the valence band (the highest occupied band) and the conduction band (the lowest unoccupied band). [12] For an electron to move from the valence band to the conduction band, it needs an energy larger or equal to the energy band gap. [12] A semiconductor's band gap is larger than the band gap of a conductor but smaller than the band gap of an insulator (Figure 2.1).

The most common semiconductor material used in solar cells is silicon. [13] When photons hit the surface of the semiconductor material, some of the photons are absorbed by the material. To be absorbed, the photon should carry sufficient energy to excite the electrons in the active layer. [12] The photon energy is transferred to the electrons in the material, causing them to become excited and move to higher energy levels. The energy from absorbed photons can break electron-hole pairs in the semiconductor. Electrons are negatively charged particles, while holes are the absence of electrons and carry a positive charge. The generation of these electron-hole pairs creates an imbalance of charges in the material. [12]

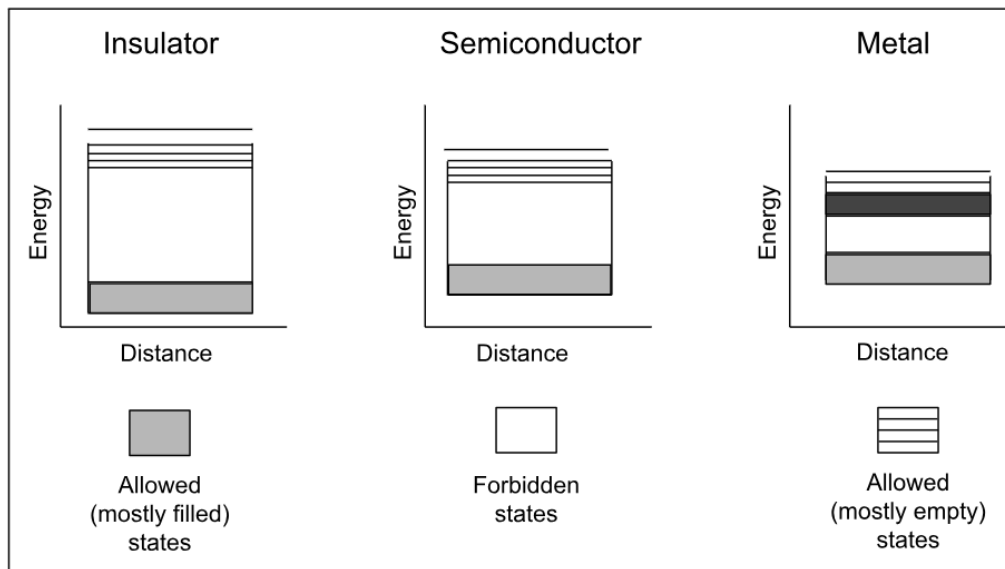


**Figure 2.1.** Band structures of insulator, semiconductor and metal, adapted from [11]

To create usable electric current, electron-hole pairs need to be separated before they recombine. The process of charge separation ensures that electric flow can be generated between two electrodes. The electric field created by the doping of the semiconductor material helps in charge separation. Electrons move towards the n-doped side which has an excess of electrons, and holes move towards the p-doped side which has a deficiency of electrons, creating a charge imbalance that can be harnessed as electric current. [14]

In a properly designed PV device, there is an electric field formed due to how the semiconductor material is doped. [12] Small amounts of other materials are introduced to modify the electrical properties of the semiconductor, which is so-called doping. This electric field also prevents the free movement of electrons and holes. [11] Due to the electric field, the negatively charged electrons are pushed towards the n-doped side of the material, while the positively charged holes are pushed towards the p-doped side of the material. This separation of charges creates a voltage difference between the two sides of the material. [14] If an external electrical circuit is connected between the n-doped and p-doped sides, the separated charges can flow through the circuit, creating an electric current. [12] Modern PV devices strive to maximize the amount of absorbed sunlight that gets converted into electricity while minimizing losses due to factors like reflection and recombination of electron-hole pairs.

The basic structure of a common silicon solar cell consists of an anti-reflection coating, an emitter layer (n-doped), a base layer (p-doped), a back surface layer, a p-n junction, and metal contacts. The anti-reflection coating works as a shield to reduce the amount of incoming sunlight that gets reflected off the surface of a solar cell. The emitter layer added to the front side of the solar cell is a thin layer of n-doped semiconductor material. The

base layer is a thicker layer of p-doped semiconductor material. When a solar cell absorbs photons, electron-hole pairs are generated in this layer. There is also an additional layer of doped material added to the back side of the cell. Its purpose is to minimize the recombination of electron-hole pairs at the back surface. The charge separation and recombination mechanism will be explained more in subsection 2.1.1. In a typical silicon solar cell, the photovoltaic effect occurs at the interface between the p-doped and the n-doped layers, which is called a p-n junction. Finally, there are front and back metal contacts that help provide a path for electric flow in the external circuit. [12]

### 2.1.1 Charge separation and recombination

In a solar cell, charge separation refers to the process in which the electron-hole pairs generated by the absorption of photons in the semiconductor material are split apart, creating separated charges that can contribute to an electric current. The separation of electron-hole pairs themselves cannot create a current flow between terminals. An electric field is introduced, by doping, which propels the electrons, causing an alignment with the electric field's direction. This specific velocity of electron motion is termed drift velocity. This drift velocity contributes to the generation of an electric current. [11]

To create the imbalance of charges, electrons and holes move to different contacts after separation. Both electrons and holes are affected by the internal electric field and the gradients of the quasi-Fermi energies, which is the driving force for charge separation. [14] In a solar cell, the negative terminal is formed when the electron conductivity is large and the hole conductivity is small, driving the electrons to flow. In contrast, the positive terminal is formed when the hole conductivity is large and the electron conductivity is small. [14] To have a working p-n junction, the electron contact has the n-type doping, and the hole contact has the p-type doping, creating a difference in concentrations between electrons and holes. [14]

On the other hand, charge recombination refers to separated electrons and holes neutralizing each other's charges and releasing energy in the form of heat or light. Recombination is detrimental to the efficiency of a solar cell because it reduces the number of charges available to contribute to the electric current, thus lowering the overall power output. There are three types of recombination, which are radiative, non-radiative, and trap-assisted recombination. In radiative recombination, electrons and holes recombine, emitting a photon of light. Some energy is lost in light form instead of being converted into electricity. Non-radiative recombination involves the direct transfer of energy from an excited electron-hole pair to lattice vibrations, releasing energy as heat. In some cases, defects or impurities in the semiconductor material can create energy levels called traps that capture charges and facilitate recombination, which is called trap-assisted recombination. [15]

To achieve high efficiency in solar cells, it is crucial to minimize charge recombination and maximize charge separation.

### 2.1.2 Characteristics and parameters

Some key characteristics and parameters collectively define solar cell performance: peak power  $P_{\max}$ , short-circuit current  $J_{\text{sc}}$ , open circuit voltage  $V_{\text{oc}}$ , and fill factor  $FF$ . The power conversion efficiency (PCE) can be derived from other factors. [16] J-V curve can be used to show the characteristics of a solar cell.

First, PSCs should be measured under standard test conditions (STC) to provide reliable results. The total irradiance should be  $1000 \text{ W/m}^2$  and the spectrum should be AM1.5 spectrum. The solar cells should also be measured at a constant temperature of  $25^\circ\text{C}$ . [16] The short-circuit current  $J_{\text{sc}}$  is the current measured in the external circuit when the electrodes are short-circuited. Both the photon flux incident determined by the incident light and the area of the cell can affect the  $J_{\text{sc}}$ . Removing the factor of area,  $J_{\text{sc}}$  typically refers to the maximum current delivered by a solar cell, which depends heavily on the optical properties of the absorber layer. [16] The open-circuit voltage ( $V_{\text{oc}}$ ) is measured when there is no current flowing through the external circuit, which refers to the maximum voltage of a solar cell. [16] Factors that can impact the  $V_{\text{oc}}$  are the saturation current density and the photo-generated current of a solar cell. Moreover, the recombination in the solar cell affects the saturation current density. Therefore,  $V_{\text{oc}}$  shows the amount of recombination in the cell. [16] Fill factor (FF) is defined as the ratio of the maximum power ( $P_{\max}$ ) generated by a solar cell and the product of  $V_{\text{oc}}$  with  $J_{\text{sc}}$ , written in Equation 2.1.1.

$$FF = \frac{P_{\max}}{V_{\text{oc}} * J_{\text{sc}}} \quad (2.1.1)$$

Using Equation 2.1.1, the fill factor can be shown as not strongly affected by the change in  $V_{\text{oc}}$ . [16] Under STC, the maximum fill factor of a typical silicon PV device can reach the range between 83 % and 85 %. [16] Finally, the power conversion efficiency is also considered when assessing a PV device. It is calculated as the ratio between the maximum generated power and the incident power as in Equation 2.1.2.

$$PCE = \frac{P_{\max}}{I_{\text{in}}} = \frac{J_{\text{mpp}} * V_{\text{mpp}}}{I_{\text{in}}} = \frac{J_{\text{sc}} * V_{\text{oc}} * FF}{I_{\text{in}}} \quad (2.1.2)$$

where  $P_{\max}$  is the maximum generated power,  $I_{\text{in}}$  is the incident current,  $J_{\text{mpp}}$  is the maximum power current density,  $V_{\text{mpp}}$  is the maximum power voltage.

External quantum efficiency (EQE) and internal quantum efficiency (IQE) are the most common parameters to quantify the cell's ability to convert photons into electrons, offering

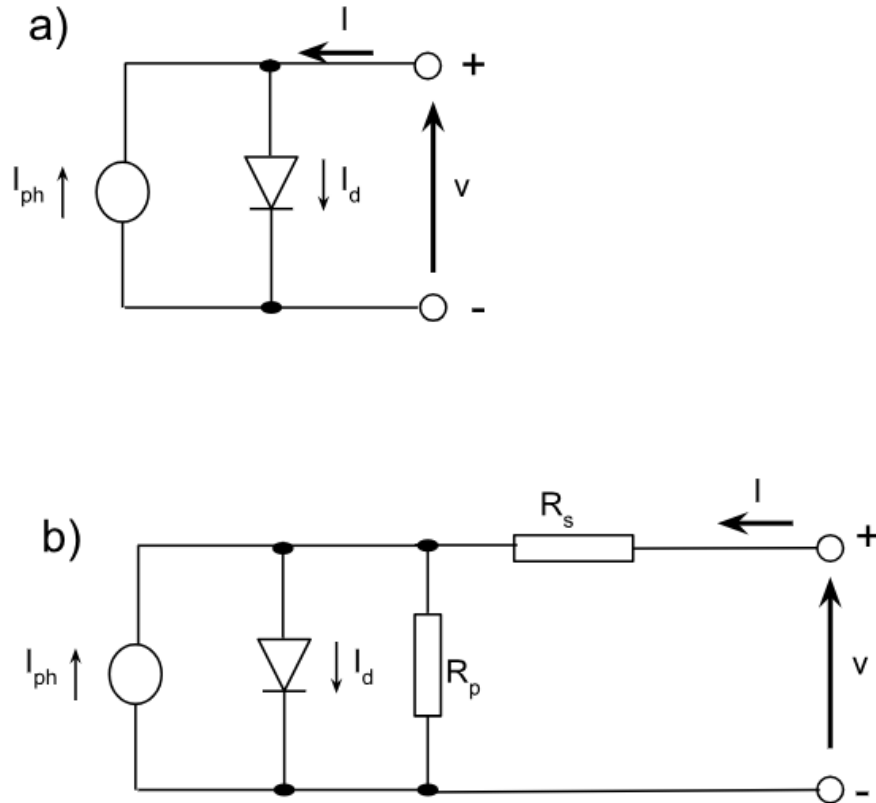


**Figure 2.2.** a) Ideal solar cell and b) Series resistance  $R_s$  and shunt resistance  $R_p$  are considered, adapted from [17].

insights into its responsiveness across the solar spectrum.[16]

When a cell behaves as the ideal diode, J-V characteristics can be written as in Equation 2.1.3:

$$J(V) = J_{rec}(V) - J_{gen}(V) - J_{ph} \quad (2.1.3)$$

where  $J_{rec}(V)$  illustrates the current density of recombination,  $J_{gen}(V)$  illustrates the current density of generation.[16] J-V characteristics can be illustrated as a simple equivalent circuit and the diode is formed by the p-n junction (Figure 2.2).

However, the FF is affected by parasitic resistances: series resistance  $R_s$  and shunt resistance  $R_p$ . When the series resistance and the shunt resistance are taken into account, the J-V characteristic of the equivalent circuit is shown in Equation 2.1.4 and Figure 2.2b).

$$J = J_0 * \left\{ \exp\left[\frac{q * (V - A * J * R_s)}{k_B * T}\right] - 1 \right\} + \frac{V - A * J * R_s}{R_p} - J_{ph} \quad (2.1.4)$$

where  $A$  is the area of the solar cell.[16]

Shunt resistance is an important parameter in solar cell characterization that quantifies the tendency of a solar cell to develop unintentional electrical paths or short circuits that bypass the intended current flow path. When shunt resistance decreases, it creates a low-resistance path for the current to flow around the active solar cell area. This effectively bypasses the photogenerated current, leading to a reduction in the cell's output current and, consequently, its overall efficiency. Shunt resistance is inversely proportional to the shunt leakage current. If the shunt resistance is too low, it can result in a phenomenon known as "shunting," which lowers the fill factor and overall power output of the solar cell.<sup>[18]</sup> In practical terms, a lower shunt resistance can result from defects or damage in the cell's semiconductor materials, improper manufacturing processes, or exposure to environmental stresses such as humidity, temperature fluctuations, or mechanical stress. Monitoring and maintaining shunt resistance within an acceptable range is crucial for ensuring the stable and efficient operation of solar cells, as lower shunt resistance can lead to performance degradation and reduced energy conversion efficiency.<sup>[18]</sup>

### 2.1.3 Stability of devices

The stability of solar cells, a crucial aspect in assessing their long-term viability, refers to their ability to maintain consistent and efficient performance over extended periods under various environmental conditions. Several factors can impact solar cell stability, which can be classified into extrinsic and intrinsic factors. Perovskite is known to inherently possess many degradations at the device level, directly caused by exposure to environmental extrinsic factors such as moisture, UV light, heat, and outside air.<sup>[9]</sup> Extrinsic factors that cause degradation in PSC concern the failures of sealing and moisture-blocking layers, which can be excluded by applying advanced encapsulation techniques.<sup>[9]</sup> <sup>[19]</sup> Intrinsic stability issues, which refer to the chemical and structural stability of PSC under various environmental conditions, are more strenuous to tackle because they cannot be solved thoroughly by improving device engineering.<sup>[19]</sup> Crystallization instability, material disintegration, or electrode instability can be caused under normal conditions. Even when the water and oxygen factors disappear, the intrinsic deterioration by thermal stress or illumination can cause degradation.<sup>[9]</sup>

As discussed above, perovskites are inherently sensitive to oxygen and moisture. Therefore, PSCs still have obstacles to being manufactured on a big scale without affecting their stability and efficiency. Fabrication of high-efficiency PSCs must be carried out in an inert environment, where oxygen and moisture levels are monitored carefully.<sup>[9]</sup> As a result, there is a gap between the PCE of PSCs in laboratory conditions and the PCE of PSCs exposed to outdoor conditions.<sup>[20]</sup> Besides the effects of moisture and oxygen, PSCs also face deterioration simply caused by light exposure.<sup>[9]</sup> Under air and UV radiation exposure, the halide perovskite materials can decompose and produce  $I_2$  with a brown

color.[21] Thermal instability of PSCs can also cause degradation because perovskites cannot withstand high temperatures.[9]

One solution to improve the intrinsic stability of PSCs is finding the optimal carrier transport materials since they notably impact the device stability and performance.[9] Hydrophobic hole transport material (HTM) and dopants were reported to increase the stability of PSC tremendously.[9] [22] 2, 2', 7, 7'-Tetrakis[N, N-di(4-methoxyphenyl)amino]-9,9'-spirobifluorene (spiro-OMeTAD) employed with lithium compound LiTFSI has shown an increment in the PSC stability.[9] Moreover, the effect of the HTM layer on the device deterioration was shown to be less significant than the perovskite's intrinsic degradation.[9] Besides utilizing electrodes and hydrophobic transport materials that increase the stability of PSC, suitable fabrication techniques and increased encapsulation can also improve the stability of the device.[9] Furthermore, hole transport (HTL) and electron transport (ETL) layers have been stated to complicate the manufacturing process and damage the stability of PSC.[9] There are studies on innovative PSC structures including ETL-free and HTM-free PSCs.[9] However, excluding ETL or HTL hinders the charge transportation inside PSCs and impacts the PCE.[9]

## 2.2 Lead halide perovskite solar cells

### 2.2.1 Perovskite and perovskite solar cell (PSC)

Calcium titanium oxide ( $\text{CaTiO}_2$ ) was first discovered by a Russian scientist, Gustave Rose, in 1839.  $\text{CaTiO}_2$  was later named perovskite after the name of Russian mineralogist Lev Perovski. Perovskite also refers to compounds that share the same crystal structure as its mineral compound.[23] The structure of perovskite follows a general formula  $\text{ABX}_3$ , which is illustrated in Figure 2.3. In perovskite solar cells (PSCs), the active layer is commonly fabricated with a hybrid organo-inorganic metal halide perovskite. A can be an organic methylammonium (MA or  $\text{CH}_3\text{NH}_3^+$ ), formamidinium (FA or  $\text{HC}(\text{CH}_2)_2^+$ , or cesium ( $\text{Cs}^+$ ) cations. B can be chosen from metal-divalent ions such as lead ( $\text{Pb}^{2+}$ ), tin ( $\text{Sn}^{2+}$ ), and germanium ( $\text{Ge}^{2+}$ ). Finally, X can be an anion such as chlorine ( $\text{Cl}^-$ ), bromide ( $\text{Br}^-$ ), and iodine ( $\text{I}^-$ ). [23]

Perovskite solar cells (PSCs) have emerged as a revolutionary technology in the field of photovoltaics. However, PSC is still a recently developed technology. The origin of PSCs can be traced to 2006 when A. Kojima et al. published the pioneering work on the initial solar cell employing a perovskite-based compound,  $\text{MAPbBr}_3$ , utilized as a sensitizer on mesoporous titanium dioxide ( $\text{TiO}_2$ ) within a dye-sensitized solar cell structure.[25] This solar cell structure achieved an efficiency rate of 2.19%. In 2009, A. Kojima et al. published about the same PSC structure but substituting bromine anion ( $\text{Br}^-$ ) with iodine anion ( $\text{I}^-$ ), with a PCE of 3.81%. [26] However, the stability of that PSC was poor

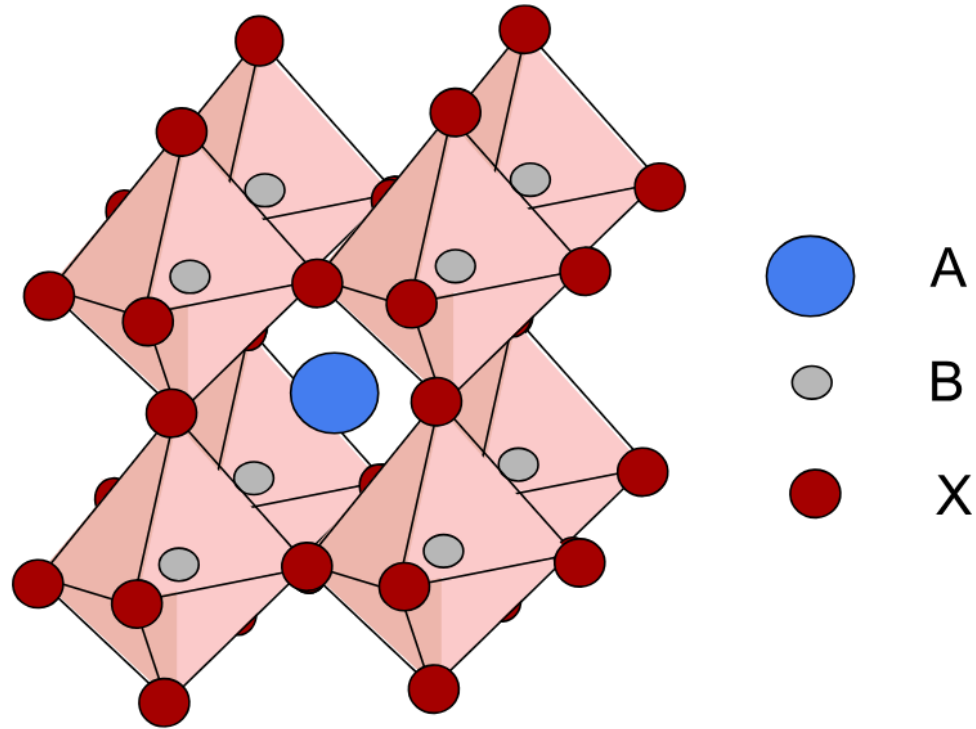


**Figure 2.3.** Structure of perovskite, adapted from [24]

because the cell contained a liquid electrolyte. Rapid advancements in perovskite solar cell technology followed, marked by a series of breakthroughs in efficiency improvements and stability enhancement. Park et al. (2011) used a similar dye-sensitized solar cell structure with quantum-dot nanomaterial, resulting in an improvement of PCE from 3.8 % to 6.5 %.[27] M. Lee, S. Henry, et al. (2012) discovered that using spiro-OMeTAD to transport the electron, resulting in PCE above 10 %.[28] Currently, the highest PCE of perovskite solar cells reached 26.1 % (Figure 2.4). Over only a decade, perovskite solar cell has had a steep increment in PCE from approximately 3 % in 2009 to over 25 % in 2019 while other PV technologies have had slower growth in PCE. The gap in PCE between PSCs and conventional Si-based cells has become closer within a relatively short period, which makes PSCs more competitive than other alternative PV technologies. [20] [29]

Perovskite has a unique crystalline structure with remarkable light absorption and charge-transport properties. [20] PSCs are not only manufactured from materials with abundant sources but also made with low-cost and unsophisticated manufacturing process, utilizing wet chemistry and simple techniques such as spin coating, dip coating, etc.[20] [30] As a thin-film solar cell, a PSC has high flexibility for various applications because it is lightweight and can be applied to many flexible substrates such as polymer. [20] Due to those advantages, PSCs have huge potential for commercialization on a large scale.[30]

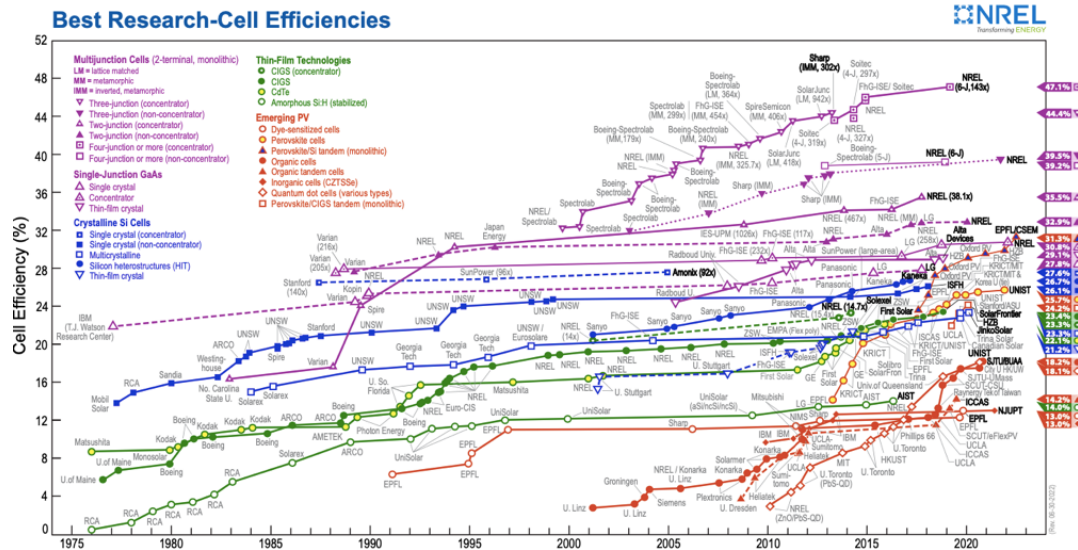


**Figure 2.4.** Plot of best research-cell efficiencies with emerging PV devices highlighted. Perovskite solar cells are illustrated by yellow dots with red outlines. This plot is courtesy of the National Renewable Energy Laboratory, Golden, CO. [29]

Currently, besides single-junction perovskite solar cells, research on perovskite tandem cells also attracts interest in the field to increase the PCE further. [23] The optical absorption of perovskite-based compounds is highly tunable. Their tunable bandgap ranges from 1.2 to 2.3 eV. [23] Researchers can test combinations of different monovalent cations, divalent cations, and halide ions. [23] The perovskite compositions with high bandgaps such as  $\text{MAPb}(\text{I}x\text{Br}_{1-x})_3$  can be used as the top cell in many tandem cells, resulting in high-PCE tandem cells. [31] [32] Recently, the low-band (below 1.5 eV) perovskites were tested and studied as the bottom cells for perovskite-perovskite tandem cells. [17] Perovskite tandem solar cells possess ultra-high PCEs of more than 30 % (Figure 2.4). [33] Although perovskite tandem cells have fascinating PCEs, their manufacturing process is challenging because of complex electrical and optical designs. [23]

There are many obstacles that prevent PSCs from commercialization. Perovskite solar cells are known to suffer from issues related to stability and durability over time. They can degrade when exposed to many external factors such as moisture, heat, oxygen, and light, which can limit their lifespan and practicality for long-term use in real-world environments. [20] [34] PSC degradation was discussed further in section 2.1.3. When PSCs are exposed to oxygen and high temperatures, they typically degrade faster. [34] One solution to alleviate the impact of external factors on PSCs is encapsulation in suitable materials. [20] [34] However, encapsulation raises the manufacturing cost without protecting PSCs completely from all external factors. [20] During the manufacturing process, PSCs might have intrinsic defects such as impurities in perovskite crystallization, which might affect the performance of PSCs. [34] Because PSCs have to cope with many challenges affecting their PCE, a noticeable concern for PSCs to compete with other solar cells in the

market is their relatively short lifespan.<sup>[34]</sup> Nowadays, the lifetime of conventional silicon-based solar cells in the market is approximately 25 years.<sup>[20]</sup> PSC's lifespan range lasts for a much shorter span - a few days or months.<sup>[20]</sup> Moreover, some PSCs contain lead including the most common structure lead-halide PSCs, which raises concerns about their potential environmental and human health impacts. Efforts are being made to develop lead-free alternatives, but addressing toxicity remains an important consideration for the technology's viability.<sup>[20]</sup>

### 2.2.2 Mesoporous and planar structures in perovskite solar cell

Currently, there are three popular types of structural configurations of PSC, which are mesoporous, conventional (n-i-p) planar and inverted (p-i-n) planar (Figure 2.5). In 2009, the structure of PSC was inspired by the conventional dye-sensitized solar cells (DSSCs), utilizing the liquid electrolyte.<sup>[26]</sup> The liquid electrolyte affected the stability of the device, which has led to advances in solid-state hole transport material (HTM).<sup>[23]</sup> In a mesoporous PSC, the perovskite layer is deposited on top of a mesoporous scaffolding that covers the electron transport layer (ETL). To improve the absorption of devices further and mitigate the direct shunts between terminals, the thickness of the absorber layer could be increased.<sup>[23]</sup> As a result, the "regular" structure of PSC (or mesoporous PSC) was developed from a meso-superstructure configuration but the perovskite layer is thicker and denser.<sup>[23]</sup> In a traditional perovskite solar cell, the perovskite layer is typically deposited on a flat substrate. However, in a mesoporous perovskite solar cell, the substrate is modified to have a highly porous structure, often resembling a scaffold or matrix of interconnected nanopores.<sup>[35]</sup> This structure enhances the overall efficiency and stability of the solar cell by providing a larger surface area for perovskite material deposition, improving charge transport, and mitigating some of the challenges associated with standard perovskite solar cells.<sup>[23]</sup> Titanium dioxide (TiO<sub>2</sub>) is the most commonly used material for scaffolding and ETL in PSCs but other metal oxides such as ZnO and SnO<sub>2</sub> can also be utilized.<sup>[28]</sup> The majority of state-of-the-art mesoporous PSCs achieved high PCEs (over 20 %), which attracts more research on PSCs and other structural designs of PSCs.<sup>[23]</sup>

In planar solar cells, the mesoporous scaffolding is removed to simplify the fabrication process.<sup>[23]</sup> PSC can work without mesoporous scaffolding because of the low exciton binding energy and long diffusion lengths of charge carriers in the devices. Thanks to that intrinsic property, excited electrons and holes have sufficient time to transport to the interfaces (HTL and ETL).<sup>[23]</sup> <sup>[28]</sup> The structure of planar solar cells consists of a transparent conductive oxide (TCO), a n-type electron transport material (ETM), a perovskite layer, a p-type hole transport material (HTM), and a metal anode. The main difference between conventional (n-i-p) planar structure and inverted (p-i-n) planar structure is that the order of ETL (n) and that of HTL (p) are switched, which affects the absorption of the perovskite

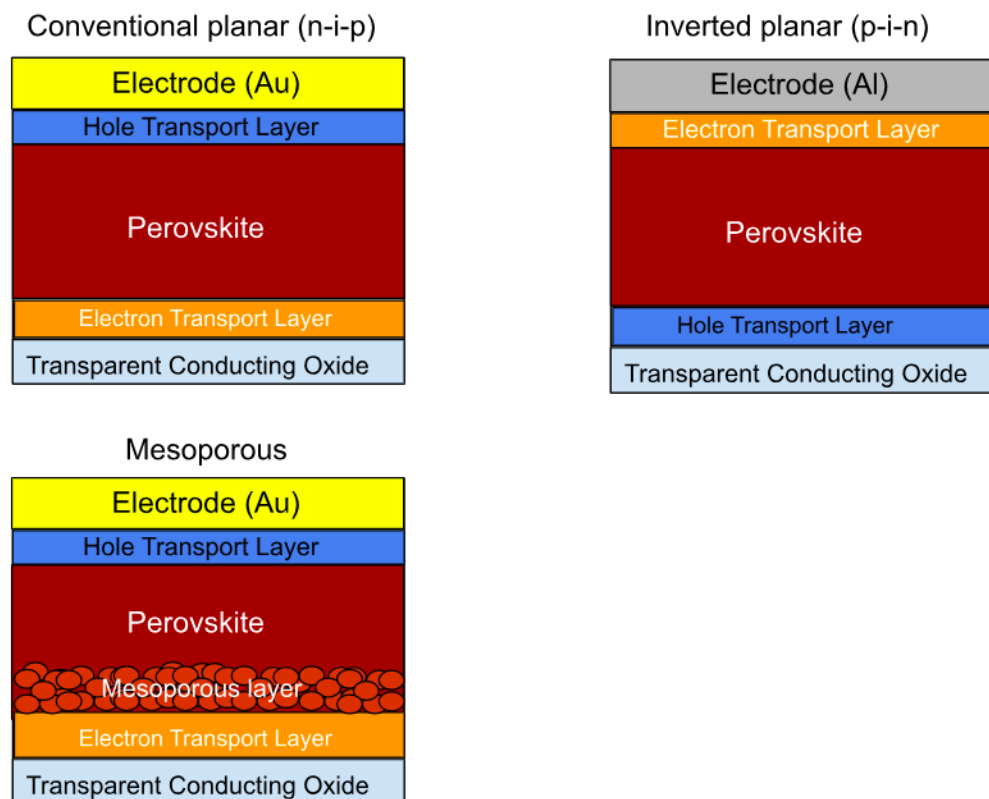


**Figure 2.5.** Schematic of conventional planar (*n-i-p*), inverted planar (*p-i-n*) and mesoporous structures of PSC, adapted from [36].

layer.[23] Planar PSC structure was first studied in 2012 with perovskite-based material  $\text{MAPbI}_3-x\text{Cl}_x$ , resulting in a PCE of only 1.8 %.[28] Poor performance might be caused due to incomplete film coverage that led to shunts.[23] Later, many studies focused on improving perovskite film smoothness and the overall processing conditions, resulting in PCEs of approximately 20 %.[37] [38] Planar heterojunction devices also have high stability, which makes the planar device structure a promising option for PSC commercialization.[37] The inverted planar structure (*p-i-n*) was adopted from the organic photovoltaic devices. State-of-the-art inverted planar PSCs have an excellent photon-to-photon conversion rate, resulting in PCE improvement. The performance of inverted planar structure also improved due to advances in perovskite fabrication techniques.[23] Moreover, the stability of inverted planar PCE is enhanced with approximately 90 % PCE after 30 days of exposure to the ambient condition.[23]

### 2.2.3 Electron transport layer

As discussed earlier in section 2.1, the electron transport layer plays a crucial role in facilitating the movement of electrons generated by light absorption in the perovskite absorber layer. First, the perovskite layer absorbs light and generates excitons (electron-

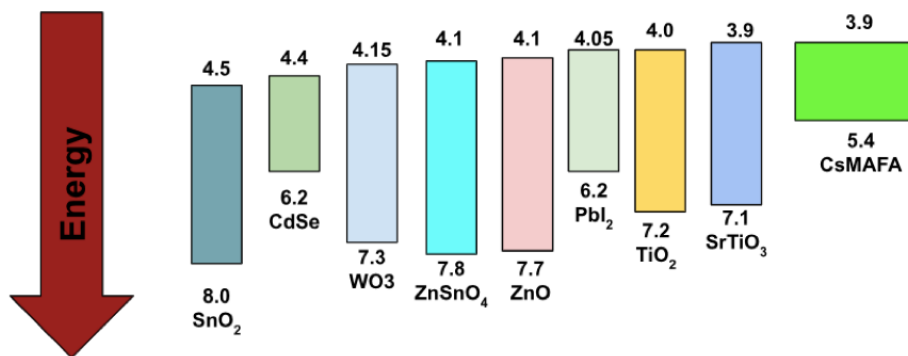


**Figure 2.6.** Illustration of band energy of different ETL with respect to perovskite, adapted from [39].

hole pairs). [12] Electrons are excited to a higher energy level, creating free electrons and positively charged holes. The goal is to separate charges and efficiently collect the electrons to generate an electric current. [12] The ETL helps to efficiently transport these electrons from the perovskite layer to the electrode. It requires ETL to have the lowest unoccupied molecular orbital (LUMO) and highest occupied molecular orbital (HOMO) higher than the active layer. [39] In other words, ETL must fulfill band alignment with the perovskite layer (Figure 2.6). Additionally, ETL must exhibit strong transmittance within the UV-Vis spectrum, allowing photons to easily traverse and be absorbed by the absorber layer. [39]

ETL is typically made of metal oxides that have high electron mobility such as TiO<sub>2</sub>, SnO<sub>2</sub>, ZnO, SiO<sub>2</sub>, and ZrO<sub>2</sub>. Different materials have unique advantages for improving PCE. [39] The ETL serves as a barrier for holes generated in the perovskite layer, which prevents the recombination of electron-hole pairs. Core-shell nanoparticles ETM were known for charge retardation. [39] There are also studies showing that doped ETM improves PCE by tuning the band gap and Fermi level, which affects the open circuit voltage. The Fermi level can be increased by using n-type doping in transition metal oxide ETM. As a result, electrons can have smooth injection from the perovskite layer. [39] Snaith et al. have studied the stability of ss-DSSC and PSC, resulting in the band diagram of different ETMs (Figure 2.6).

Despite being the most well-known design for PSC, a TiO<sub>2</sub>-based PSC was suggested to have lower stability than a TiO<sub>2</sub>-free PSC. A PSC with ultra-thin amorphous TiO<sub>x</sub> has achieved higher stability in electronic properties than a PSC with mesoporous TiO<sub>2</sub>. [39] Cadmium selenide (CdSe) nanocrystal ETM has shown a strong PL quenching effect, which enhances better charge separation and recombination resistance. PSC with ETL made from CdSe achieved a PCE up to 11.7%. [39] SnO<sub>2</sub> nanoparticle ETM, which is studied in this thesis, addressed many drawbacks of TiO<sub>2</sub> ETM in PSC. Mesoporous TiO<sub>2</sub> PSCs with high PCEs require high temperatures in the manufacturing process, which

hinders their commercialization and flexibility.<sup>[39]</sup> While planar-type PSCs can be fabricated without high temperatures, they usually face hysteresis issues.<sup>[39]</sup> Planar SnO<sub>2</sub>-based PSCs can be fabricated with a low-temperature simple process, resulting in almost hysteresis-free devices.<sup>[39]</sup> The advantages of SnO<sub>2</sub> nanoparticles ETM over TiO<sub>2</sub> ETM in PSC will be discussed further in section 3.1.

### 3. MATERIALS AND METHODS

This chapter focuses on the experimental part of this thesis, delving into the manufacturing process of solar cells. First, the tin-oxide-based electron transport material will be introduced, and then the materials and methods used in the fabrication process of perovskite solar cell (PSC) will be discussed. Finally, the devices and measurements to analyze solar cell's performance and characterization are described.

#### 3.1 Tin-based electron transport material

The electron transport material studied in this thesis was nanoparticle  $\text{SnO}_2$ . The fabrication of the electron transport layer was realized by following the work of the Institute of Semiconductors, Chinese Academy of Sciences, Beijing, China.<sup>[37]</sup> In addition, the method used by The Centre for Hybrid and Organic Solar Energy (CHOSE) in Italy was tested.

Traditionally, titanium-based electron transport material ( $\text{TiO}_2$ ) is used in lead-based perovskite solar cells. However, planar titanium-based structure usually shows hysteresis and lower stability compared to mesoporous structure.<sup>[37]</sup> Despite of high PCE, one noticeable disadvantage of mesoporous titanium-based structure is the sintering process at high temperature (over  $450^\circ\text{C}$ ).  $\text{SnO}_2$  has a deeper conduction band than traditional  $\text{TiO}_2$  (Figure 3.1), which increases the electron mobility between the perovskite layer and electron transport layer (ETL). The  $\text{SnO}_2$  colloidal film has much higher mobility than  $\text{TiO}_2$  film when measured utilizing space-charge-limited current (SCLC) model.<sup>[37]</sup> In addition, the  $\text{SnO}_2$  nanoparticles are highly crystallized, which minimizes the number of defects on the ETL.<sup>[37]</sup>

Planar  $\text{SnO}_2$ -based devices can be easily manufactured at low temperature ( $150^\circ\text{C}$ ) with high electron mobility and enhanced charge transfer from perovskite layer to ETL. The tin-based devices also have insignificant hysteresis and high stability, which is competitive advantage in manufacturing low-cost and stretchable devices. Previously,  $\text{SnO}_2$  has been tested as the electron transport layer in organic solar cells and dye-sensitized solar cells. Recently, planar  $\text{SnO}_2$ -based perovskite solar cells were reported with the PCE around 19.9 % and negligible hysteresis.<sup>[37]</sup> The PCE of low-temperature-processed planar  $\text{SnO}_2$ -based devices can reach over 20 % with high stability.<sup>[41]</sup> Electron transport

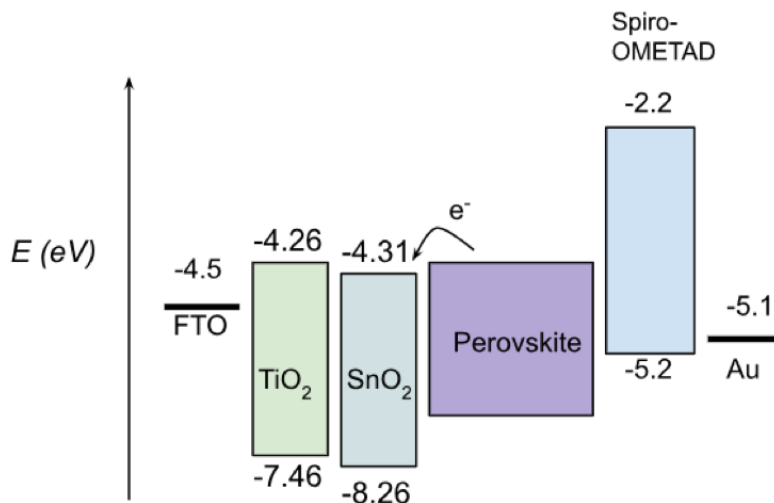


**Figure 3.1.** Band alignment of  $\text{TiO}_2$ ,  $\text{SnO}_2$  and perovskite layer due to different conduction bands, adapted from [40]

layer fabricated from  $\text{SnO}_2$  nanoparticles may become the future for the large-scale production of perovskite solar cells.

## 3.2 Solar cell manufacturing

In this thesis, the standard n-i-p solar cell structure is used, following a protocol of the Hybrid Solar Cells (HSC) team, Tampere University. The procedures are described in detail, individually discussed within sub-chapters 3.2.1 to 3.2.4, focusing on each layer of the fabrication process.

### 3.2.1 Substrate and electrodes

Patterned fluorine-doped tin oxide (FTO) and indium tin oxide (ITO) glass substrates from OPV Tech were used. Glass substrates were marked on the glass sides to distinguish them from the FTO/ITO sides. In the first step, the substrates were cleaned with a soft brush and 2 % Mucasol solution, then rinsed with ultrapure water (milliQ water). The substrates were sonicated in an ultrasonic bath in milliQ water, acetone, and 2-propanol sequentially. Each sonicating step lasted for 15 minutes. After sonication, substrates were dried with  $\text{N}_2$  flow. Cleaned substrates were stored in clean Petri dishes sealed with parafilm until the next step. Before depositing the electron transport layer, substrates underwent UV- $\text{O}_3$  treatment for 30 minutes.

After the deposition of all other layers in the solar cell, the top electrode made of gold (Au) was formed by evaporating gold onto substrates using vacuum deposition with the assistance of a metal mask. This technique allows creating thin films with specific patterns and

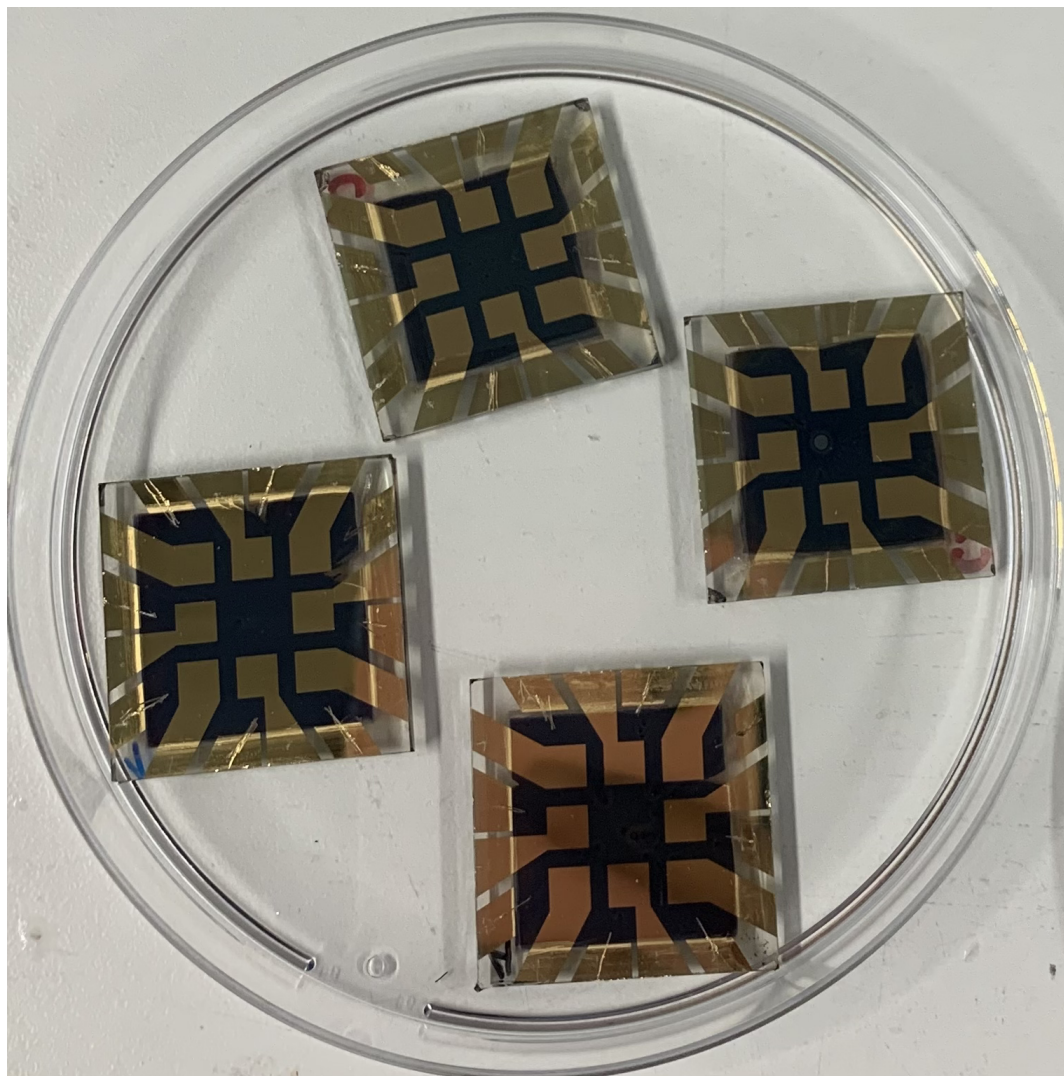


**Figure 3.2.** Finished solar cell samples.

precise control over the thickness. First, the sides of the sample were wiped with DMSO, and dried with  $N_2$  flow, to expose electrodes. Scratches were made on the substrate's surface to have conductivity when measuring samples later. The samples were placed in a mask that covered specific areas of samples. The masked samples were placed in a rotating holder within the vacuum deposition apparatus (MBraun Optivap). To begin the deposition process, small particles of gold (Au) weighing between 550-600 mg were placed in a small holder located beneath the samples. The pressure inside the sealed chamber was reduced to a vacuum level of approximately  $5 \cdot 10^{-6}$  mbar. The gold material was vaporized and the rate of evaporation was gradually increased until the gold layer reached a thickness of 100 nm approximately. The final appearance of the substrates can be seen in Figure 3.2. The complete samples were stored in a dry cabinet until they were measured. Ideally, the samples should rest overnight before their first measurement.

|            |     |     |     |     |       |
|------------|-----|-----|-----|-----|-------|
| Ramp (min) | 5   | 15  | 5   | 5   | 5     |
| Temp (°C)  | 125 | 325 | 375 | 450 | 150   |
| Hold (min) | 5   | 5   | 5   | 30  | 9.999 |

**Table 3.1.** Standard sintering procedure

### 3.2.2 Electron transport layer

In this work, solar cells that contain both compact (c-TiO<sub>2</sub>) and mesoporous titanium dioxide (m-TiO<sub>2</sub>) layers were used as a reference to compare with solar cells that have SnO<sub>2</sub> layer as ETL. The c-TiO<sub>2</sub> layer was deposited via spray pyrolysis. The initial solution was created by mixing 1.15 ml of the stock solution of titanium diisopropoxide bis(acetylacetonate) (diluted to 75 % in 2-propanol) with 4.95 ml of 2-propanol. The oven was heated to 450 °C. After that, the precursor was sprayed on the substrates with a spray gun steadily 12-13 times with 20 seconds between each spray cycle. To get a uniform coating, the spraying direction was changed for each spraying cycle reversely. The bases were heated at 450 °C for 10 minutes with the oven door open and for 45 minutes with the oven door closed.

Spin-coating technique was used to deposit the m-TiO<sub>2</sub> layer. Initially, a solution of TiO<sub>2</sub> Paste 30 NRD (Greatcell Solar) in ethanol, with a concentration of 150 mg/mL, was prepared. The paste was stored in a sealed container and kept in magnetic stirring overnight. The stirring should be sustained until utilization because the paste should be well dissolved. Before spin-coating, the edges of the substrate were taped to protect them from the m-TiO<sub>2</sub> precursor. After placing the substrate on the spin coater, 80 µl of the prepared solution was dispensed onto the substrates. Substrate was then spun for 10 seconds at a rate of 4000 rpm with an acceleration of 2000 rpm/s. Following the spin coating, the substrate was placed on a hot plate at 100 °C for a brief period. Subsequently, the substrates were transferred to an oven and underwent a sintering process outlined in Table 3.1. After the sintering, the substrates were transferred to a glovebox while they were still approximately 150 °C to prevent moisture infiltration into the pores.

For SnO<sub>2</sub>-based solar cells, SnO<sub>2</sub> film was also deposited using spin coating method. In this work, two different concentrations of SnO<sub>2</sub> were tested: 2.67 % and 7.5 %. First, SnO<sub>2</sub> solutions were prepared from SnO<sub>2</sub> 20 % stock solution by diluting with deionized H<sub>2</sub>O and mixed well before usage. After placing the substrates on the spin coater's holder, 50 µl SnO<sub>2</sub> solution was pipetted onto the substrates. The spin coating time was 32 seconds (2 seconds delayed at the beginning of the program) at a rate of 3000 rpm with a ramp of 588 rpm/s. When the program ended, substrates were annealed for 30 minutes on a hot plate at 150 °C. After letting the substrates cool down for a few moments, substrates were stored in clean plastic Petri dishes and transferred into the glovebox.

| Dopants | Mw (g/mol) | Solvent      | c (mg/mL)<br>(M (mol/L)) | Equivalent to spiro $mL_{\text{additive}}/mL_{\text{spiro}}$<br>$(mol_{\text{additive}}/mol_{\text{spiro}})$ |
|---------|------------|--------------|--------------------------|--|
| FK209   | 1503.18    | Acetonitrile | 300 (0.2)                | 14.5 (0.1)   |
| Li-TFSI | 287.09     | Acetonitrile | 520 (1.8)                | 8.8 (0.53)   |
| tBP     | 135.21     |              |                          | 14.4 (3.2)   |

**Table 3.2.** Information about the amounts of dopants.

### 3.2.3 Perovskite layer

The next layer in the manufacturing process is the perovskite layer, which was fabricated within the inert atmosphere in the glovebox. The composition of the perovskite was  $\text{Cs}_{0.05}(\text{MA}_{0.17}\text{FA}_{0.83})_{0.95}\text{Pb}(\text{I}_{0.83}\text{Br}_{0.17})_3(\text{CsMAFAPb})$ . CsI stock solution in DMSO with a concentration of 1.5 M was prepared beforehand and can be used for up to 4 weeks. The newly made stock solution was stirred at 60 °C overnight and then stirred at 60 °C for 10-15 minutes before use to dissolve solids completely when making perovskite precursor. To prepare the precursor 110.3 mg formamidinium iodide (FAI), 14.4 mg methylammonium bromide (MABr), 342.3 mg lead(II) iodide ( $\text{PbI}_2$ ), 49.6 mg lead(II) bromide ( $\text{PbBr}_2$ ) were dissolved in 135  $\mu\text{L}$  DMSO, 540  $\mu\text{L}$  DMF. After all the solids were dissolved, 27  $\mu\text{L}$  CsI stock solution was added to the precursor. The precursor solution underwent continuous magnetic stirring overnight.

The spin coating program used in this work has a speed of 1000 rpm and a ramp of 200 rpm/s for the first 10 seconds, and a speed of 6000 rpm and a ramp of 2000 rpm/s for the last 20 seconds. The total running time of the program is 35 seconds. To deposit the perovskite layer, 75  $\mu\text{L}$  of the precursor was dispensed onto the substrate and the program started immediately with an open spin coater lid. 100  $\mu\text{L}$  of chlorobenzene was added 5 seconds before the program ended. The perovskite films should be smooth visibly. The substrates were annealed on a hot plate at 110 °C for an hour.

### 3.2.4 Hole transport layer

The hole transport material (HTM) used in this thesis was 2,2',7,7'-Tetrakis[N, N -di(4-methoxyphenyl)amino]-9,9'-spirobifluorene (spiro-OMeTAD). First, the spiro-OMeTAD solution was prepared with a concentration of 28.4 mM in chlorobenzene. The solution was mixed at 60 °C for a few minutes to dissolve all the spiro-OMeTAD. After the temperature of the solution decreased, the dopants were added with amounts in Table [3.2](#).

In this study, 36.8 mg of spiro-OMeTAD was dissolved in 1018  $\mu\text{L}$  of chlorobenzene. After all spiro-OMeTAD solids were dissolved, 14.65  $\mu\text{L}$  tBP, 8.91  $\mu\text{L}$  Li-TFSI and 14.76  $\mu\text{L}$  FK209 were added to the solution respectively. The final solution was stirred well with a

magnet before usage. The HTM should be deposited on substrates immediately after the perovskite films cool down from annealing. Dynamic solution deposition was used with the speed of 200 rpm for 1.8 seconds and the speed of 1800 rpm for 30 seconds. 80  $\mu$ l of Spiro solution was dispensed onto substrates dynamically. After the film was formed, substrates rested overnight in a dry cabinet.

### 3.2.5 UV Ozone (UVO) treatment

In this study, ultraviolet-ozone (UVO) treatment was used for reprocessing substrates before spin-coating SnO<sub>2</sub> nanoparticle solution onto them. There have been many studies about the effect of UVO treatment on the performance of perovskite solar cells. [37] [42] [43] By improving the quality of interface between ETL and perovskite layer, the charge transport is enhanced, leading to improved PCE. UV irradiation enhances performance of solar cells by creating concentrated surface states. Ozone (O<sub>3</sub>) is highlighted as a potent oxidizing agent. The combination of UV and ozone (UVO) treatment is effective in removing contaminants from electronic substrates and modifying electrode properties. Proper UVO treatment on FTO TiO<sub>2</sub>-based perovskite solar cell can improve the average PCE by approximately 20 % from 14.5 % to 17.4 % with 15-minute UVO treatment. [42] Q. Jiang et al. (2016) also utilized 30-minute UVO treatment in the manufacturing process of SnO<sub>2</sub>-based perovskite solar cells, resulting in highly efficient and stable solar cells. [37]

## 3.3 Efficiency and stability measurement

In this part, solar cell characterization and performance testing are explained. Testing metrics such as J-V and quantum efficiency used to study solar cell efficiency and stability in this study will be introduced.

### 3.3.1 J-V measurement

In the photovoltaic (PV) devices field, J-V measurements serve as an indispensable tool for researchers to guide the optimization and quality control of solar cells to drive advancements in sustainable energy technology. J-V (current-voltage) measurement is a crucial and widely employed technique in the realm of solar cell testing and characterization. This method provides valuable insights into the performance and efficiency of photovoltaic (PV) devices by revealing their electrical behavior under varying external conditions. The J-V curve is generated by varying the voltage bias across a solar cell and measuring the resulting current flow (Figure 3.3). Critical parameters such as open-circuit voltage ( $V_{oc}$ ), short-circuit current ( $J_{sc}$ ), fill factor (FF), and overall power conversion efficiency (PCE) can be assessed via this measurement. Maximum power point (MPP) is achieved where the product of the voltage and current is highest. In practical terms, finding and operating

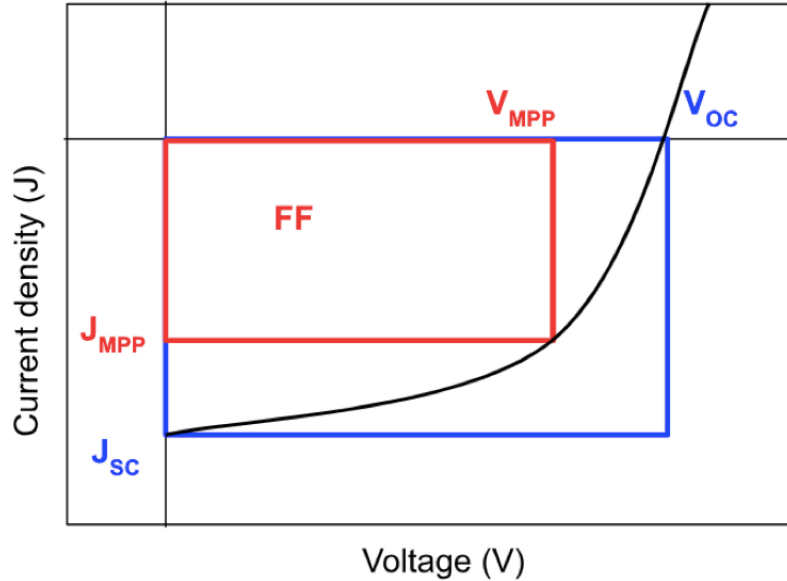


**Figure 3.3.** A typical J-V curve with short-circuit current ( $J_{sc}$ ), open-circuit voltage ( $V_{oc}$ ), fill factor (FF), and maximum power points (MPP), adapted from [44].

at the maximum power point is crucial for maximizing the energy conversion efficiency of a solar cell. Solar power systems often incorporate tracking algorithms or hardware to continuously adjust the operating point to the MPP as environmental conditions change throughout the day. This ensures that the system extracts the most energy possible from the available sunlight, leading to higher overall energy production. [45] In this thesis, the current density-voltage (J-V) curve of a solar cell should be measured the day after the solar cell fabrication finishes. Sinus-70 by Wavelabs, Germany was used as a solar simulator in the measurement, and its calibrated intensity was standard 1 sun ( $100 \text{ mW/cm}^2$ ). The Litos Lite parallel JV and stability measurement platform used in measuring samples was produced by FLUXiM AG, Switzerland. During stability measurement, samples were measured in the condition of inert  $\text{N}_2$  gas. Samples were scanned in both forward and reverse directions, resulting in two sweeps. The scanning range in J-V measurements was from -0.2 to 1.2 V, and the scan speed was 50 mV/s. In addition, samples were measured with metallic masks to focus on areas that needed to be measured.

### 3.3.2 Quantum efficiency measurement

Quantum efficiency (QE) measurement is a fundamental technique used to evaluate the effectiveness of photovoltaic devices in converting incident photons into electrical current. It helps assess the device's performance by providing insights into the device's response across different wavelengths of light. As a result, this measurement is important to study the behavior of solar cells under varying light conditions and to optimize the design for

enhanced energy conversion. There are internal quantum efficiency (IQE) and external quantum efficiency (EQE). These measurements are typically conducted by illuminating the device with monochromatic light of known intensity across a range of wavelengths and then measuring the resulting photocurrent. The QE is calculated as the ratio of the number of collected electrons to the number of incident photons.<sup>[44]</sup> QE measurements offer valuable information about the device's internal processes, such as carrier generation, recombination, and external factors like reflection losses and absorption characteristics. EQE focuses on the efficiency of carrier generation within the device. IQE refers to external factors such as reflection, transmission, and absorption losses as light interacts with the device's surface and interfaces. In other words, EQE assesses how efficiently a device converts incident light into electron-hole pairs within its active material. IQE measures how efficiently a solar cell converts incident light into electron-hole pairs within its active material while considering external losses.<sup>[44]</sup> In this thesis, the measuring device used for QE measurements is Newport QuantX-300 Quantum Efficiency Measurement Solution which can measure both EQE and IQE of samples. The range of wavelength for measuring was 300-850 nm. The samples with the highest PCE were chosen to measure their QE.

### **3.3.3 Stability measurement**

For perovskite solar cells, procedures for testing stability are based on the International Summit on Organic Photovoltaic Stability (ISOS) protocols. Light soaking tests (ISOS-L) allow monitoring stability testing conditions such as constant light, atmosphere and temperature in the laboratory.<sup>[46]</sup> In this work, due to the ISOS-L-11 protocol, solar cell stability was assessed under constant illumination (1 sun under AM 1.5G condition) from the solar simulator Sinus-70 by Wavelabs, Germany. The measurement was carried out in an inert atmosphere (Nitrogen). Besides, maximum power point tracking (MPPT) was used to dynamically adjust the voltage and current, ensuring that the device consistently operates near its peak power output despite degradation. By implementing MPPT algorithms, which adjust the operating conditions of the solar cell or system to continuously maintain or approach the MPP, stability and energy production are optimized. The stability test was carried out for approximately 100 hours. The best-performing cells of the batch were chosen as samples for testing stability.

## 4. RESULTS AND DISCUSSION

In this chapter, the results from experimental work will be shown. The performance of different batches is illustrated and discussed to study the most optimal recipe and substrate for nanoparticle SnO<sub>2</sub>-based perovskite solar cells. Samples with different assumed concentrations of SnO<sub>2</sub> are discussed, then SnO<sub>2</sub>-based PSCs are compared to TiO<sub>2</sub>-based PSCs. Results of samples made from ITO and FTO are also analyzed to determine the more suitable substrate for SnO<sub>2</sub>-based PSCs. Finally, stability measurement results are shown in section 4.2.

### 4.1 Solar cell performance

Q. Jiang et al. (2016) suggested testing the concentration of nanoparticle SnO<sub>2</sub> stock solution because it might be different from what the provider stated.<sup>[37]</sup> In this study, assuming the concentration was 15 % when preparing the solution provided the best performance. The exact concentration of the stock solution was not verified experimentally as Q. Jiang et al. (2016) did in their article. As the article was published in 2016, a stock solution used in this study is from a different batch than in the article.

First, the performance of the samples with different concentrations of nanoparticle SnO<sub>2</sub> stock is discussed to test the best-assumed concentration of the stock solution. The average values of various parameters can be seen in Table 4.1 and all results of parameters are illustrated in Figure 4.1. The recipe of SnO<sub>2</sub> with the best performance was chosen for further batches. ITO was used as substrate for those samples and the parameters were calculated from the reverse sweep. Samples made with 50 µl SnO<sub>2</sub> 2.67 % from assumed 15 % SnO<sub>2</sub> stock solution resulted in higher average PCE and nearly achieved the best PCE. In addition, this type of SnO<sub>2</sub>-based PSC also showed less varied PCE values within their boxplot than the other three types, which can be seen in Figure 4.1.

The performance of solar cells with electron transport material (ETM) nanoparticle SnO<sub>2</sub> 2.67 % and 7.5 % can be compared with solar cells with ETM TiO<sub>2</sub> in Table 4.2. FTO was used as substrate in all these cells. PSCs with TiO<sub>2</sub> electron transport layer (ETL) reach the highest average and best values of parameters. However, the gap between the results of SnO<sub>2</sub>-based solar cells and TiO<sub>2</sub>-based solar cells is not tremendous. Fill factor values of SnO<sub>2</sub> 2.67 % are almost identical to TiO<sub>2</sub>. The best fill factor result of SnO<sub>2</sub>

| Recipe  | PCE(%)          | FF (%)           | $J_{sc}$ (mA/cm <sup>2</sup> ) | $V_{oc}$ (V)   | n  |
|---|-----------------|------------------|--------------------------------|----------------|----|
| 50 $\mu$ l (SnO <sub>2</sub> ) 2.67 % (assuming SnO <sub>2</sub> stock 20 %)  | 5.93<br>(10.59) | 43.65<br>(65.72) | 16.52<br>(23.28)               | 0.69<br>(1.01) | 24 |
| 50 $\mu$ l (SnO <sub>2</sub> ) 2.67 % (assuming SnO <sub>2</sub> stock 15 %)  | 8.57<br>(10.79) | 46.10<br>(55.43) | 20.22<br>(22.73)               | 0.88<br>(0.99) | 24 |
| 200 $\mu$ l (SnO <sub>2</sub> ) 2.67 % (assuming SnO <sub>2</sub> stock 15 %) | 7.72<br>(10.08) | 42.56<br>(50.69) | 19.75<br>(23.62)               | 0.88<br>(1.00) | 24 |
| 200 $\mu$ l (SnO <sub>2</sub> ) 2.67 % (assuming SnO <sub>2</sub> stock 20 %) | 8.02<br>(11.91) | 45.48<br>(71.03) | 18.13<br>(21.09)               | 0.85<br>(1.02) | 24 |

**Table 4.1.** Average and the best values of parameters for different SnO<sub>2</sub> recipes. The best values are placed in brackets.

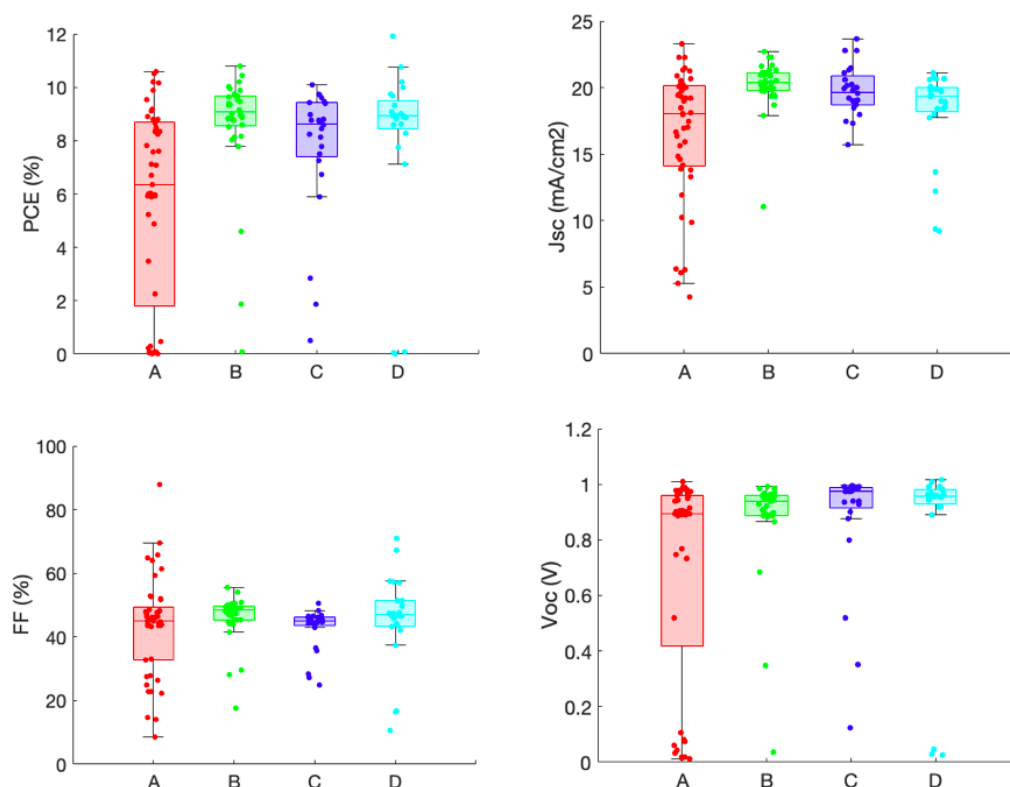


**Figure 4.1.** Boxplot of PCE, FF,  $J_{sc}$ , and  $V_{oc}$  for samples manufactured with SnO<sub>2</sub> 2.67 % assuming that the concentration of stock solution could be either 20 % or 15 %. Type A is 50  $\mu$ l SnO<sub>2</sub> 2.67 % (assuming SnO<sub>2</sub> stock 20 %). Type B is 50  $\mu$ l SnO<sub>2</sub> 2.67 % (assuming SnO<sub>2</sub> stock 15 %). Type C is 200  $\mu$ l SnO<sub>2</sub> 2.67 % (assuming SnO<sub>2</sub> stock 15 %). Type D is 200  $\mu$ l SnO<sub>2</sub> 2.67 % (assuming SnO<sub>2</sub> stock 20 %).

| Recipe                              | PCE (%)          | FF (%)           | $J_{sc}$ (mA/cm <sup>2</sup> ) | $V_{oc}$ (V)   | n  |
|-------------------------------------|------------------|------------------|--------------------------------|----------------|----|
| FTO SnO <sub>2</sub> 2.67 %         | 11.30<br>(14.60) | 56.77<br>(70.38) | 19.77<br>(23.63)               | 0.98<br>(1.05) | 56 |
| FTO SnO <sub>2</sub> 7.5 %          | 11.04<br>(15.64) | 54.37<br>(68.09) | 19.81<br>(23.54)               | 0.98<br>(1.07) | 64 |
| FTO compact + meso TiO <sub>2</sub> | 13.25<br>(17.88) | 56.76<br>(67.58) | 22.65<br>(28.51)               | 1.01<br>(1.02) | 72 |

**Table 4.2.** Average and the best values of parameters for ETM SnO<sub>2</sub> 2.67 %, SnO<sub>2</sub> 7.5 %, TiO<sub>2</sub>. The best values are placed in brackets.

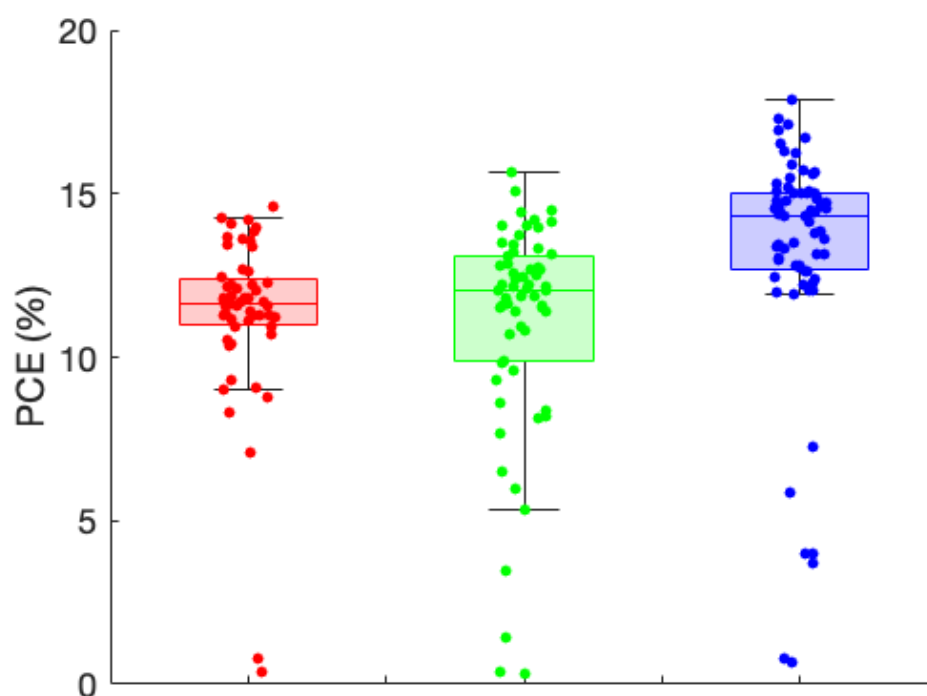


**Figure 4.2.** Boxplot of PCEs for samples manufactured with SnO<sub>2</sub> 2.67 % (red), SnO<sub>2</sub> 7.5 % (green) and TiO<sub>2</sub> (blue). The assumed concentration of nanoparticle SnO<sub>2</sub> stock was 15 %.

2.67 % type is the highest among all samples. Between two different concentrations of SnO<sub>2</sub>, samples manufactured with nanoparticle SnO<sub>2</sub> 7.5 % have a higher best PCE value compared to samples manufactured with nanoparticle SnO<sub>2</sub> 2.67 %. Nevertheless, FTO SnO<sub>2</sub> 2.67 % yields a higher average PCE value than SnO<sub>2</sub> 7.5 %. FTO SnO<sub>2</sub> 2.67 % also shows less-varied PCE values than SnO<sub>2</sub> 7.5 % and TiO<sub>2</sub> in Figure 4.2. Therefore, SnO<sub>2</sub> might be more suitable for large-scale manufacturing when the variation of batch can affect efficiency.

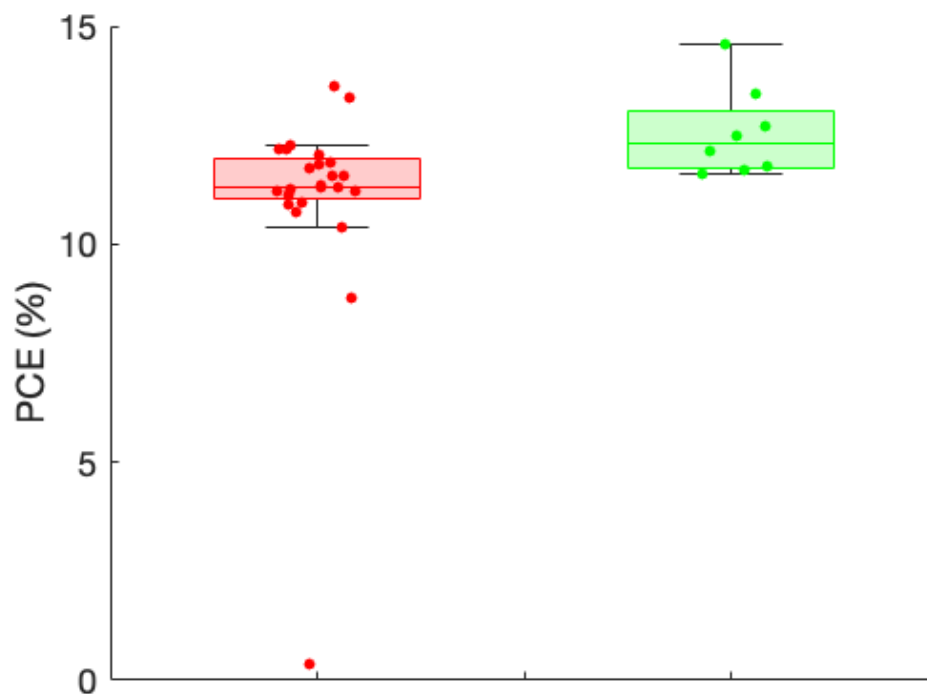


**Figure 4.3.** Boxplot of PCE values of a sample fabricated with one-week-old  $\text{SnO}_2$  2.67 % solution (green) and a sample fabricated with  $\text{SnO}_2$  2.67 % made on the same day of spin-coating (red).

Solar cells were fabricated from both fresh and 1-week old  $\text{SnO}_2$  solutions. The solar cell with ETM one-week-old nanoparticle  $\text{SnO}_2$  2.67 % solution achieved noticeably higher PCE values than the nanoparticle  $\text{SnO}_2$  2.67 % solution made on the same day of spin-coating (Figure 4.3). It would be interesting to study further the impact of the time gap between the day when making  $\text{SnO}_2$  2.67 % solution and the day when spin-coating ETL. Unfortunately, in this study, only one batch of PSCs was fabricated from one-week-old  $\text{SnO}_2$  2.67 % and compared to other  $\text{SnO}_2$  2.67 % PSCs. There might be a correlation between one-week-old  $\text{SnO}_2$  2.67 % and PCE values, which would be an interesting effect.

When comparing PCE values of samples measured after fabrication and after some time, although the results were inconsistent in different  $\text{SnO}_2$  concentrations and different batches,  $\text{SnO}_2$ -based solar cell PCE values have shown signs of improvement over time. The aim of re-measuring different batches after different periods was not to prove that  $\text{SnO}_2$ -based solar cell PCE values improve over time, but to study improvement patterns of  $\text{SnO}_2$ -based solar cells when affected by various factors. In this study, there were two batches of solar cells manufactured with  $\text{SnO}_2$  2.67 %,  $\text{SnO}_2$  7.5 % and  $\text{TiO}_2$ . The PCE values of the first batch one day after fabrication and 3 weeks after fabrication can be

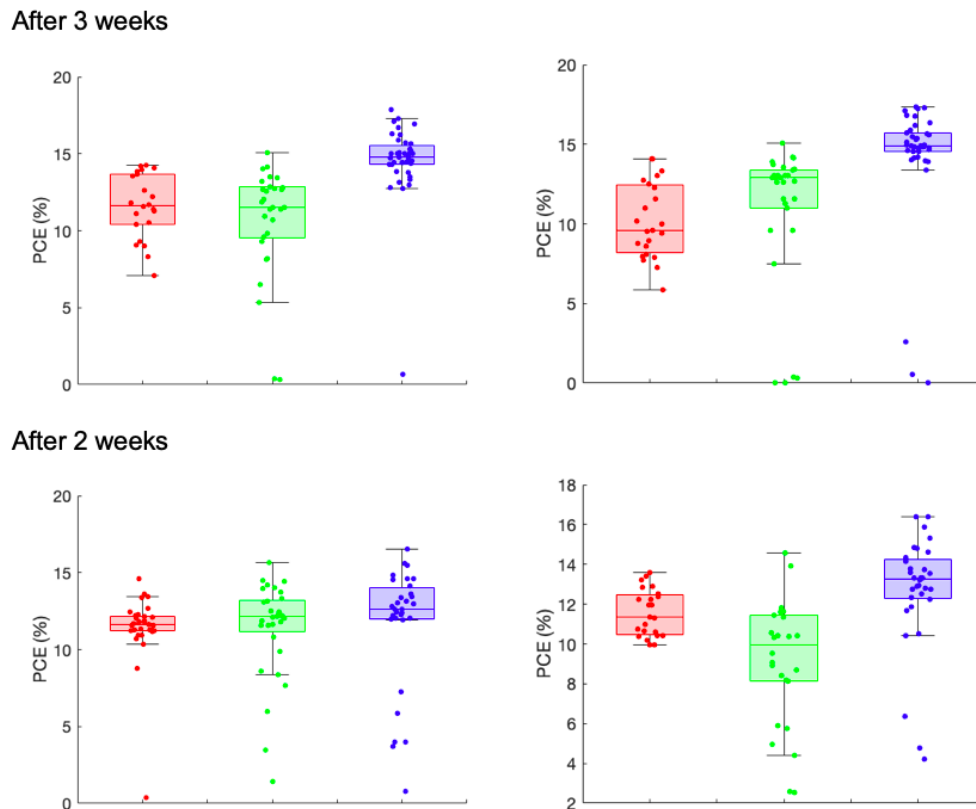


**Figure 4.4.** Boxplots of PCE values of SnO<sub>2</sub> 2.67 % (red), SnO<sub>2</sub> 7.5 % (green) and TiO<sub>2</sub> (blue) from left to right one day after fabrication (left) compared to approximately 2 weeks and 3 weeks after fabrication (right).

seen in Figure 4.4. The SnO<sub>2</sub> 7.5 % type of samples have shown noticeably improved PCE values, which shifts the boxplot and the quartile line upward. In contrast, PCE values of TiO<sub>2</sub>-based samples stayed the same after 3 weeks. Next, the PCE values of the second batch one day after fabrication and after 2 weeks are illustrated in Figure 4.4. SnO<sub>2</sub> 2.67 % has stayed more stable than SnO<sub>2</sub> 7.5 %. TiO<sub>2</sub> has also achieved higher PCE values over time, even though the improvement was not significant. Since the results were not consistent, it would be better to study the effect of time on power conversion efficiency using an adequate amount of batches that can increase the validity of the result. Even though not as stable over time as TiO<sub>2</sub> was, the sign of SnO<sub>2</sub>-based PSCs improvement over time can still be observed.

From Figure 4.5 hysteresis of best-performing samples manufactured with newly-made SnO<sub>2</sub> 2.67 %, 1-old-week ceSnO<sub>2</sub> 2.67 %, SnO<sub>2</sub> 7.5 % and TiO<sub>2</sub> can be compared. Among the four types, the sample made with newly-made SnO<sub>2</sub> 2.67 % resulted in the least hysteresis, followed by the sample made with compact and mesoporous TiO<sub>2</sub>. Even though the sample manufactured with 1-old-week SnO<sub>2</sub> 2.67 % achieved higher PCE values, its hysteresis was the biggest among the four types of PSCs. ETM SnO<sub>2</sub> 2.67 %

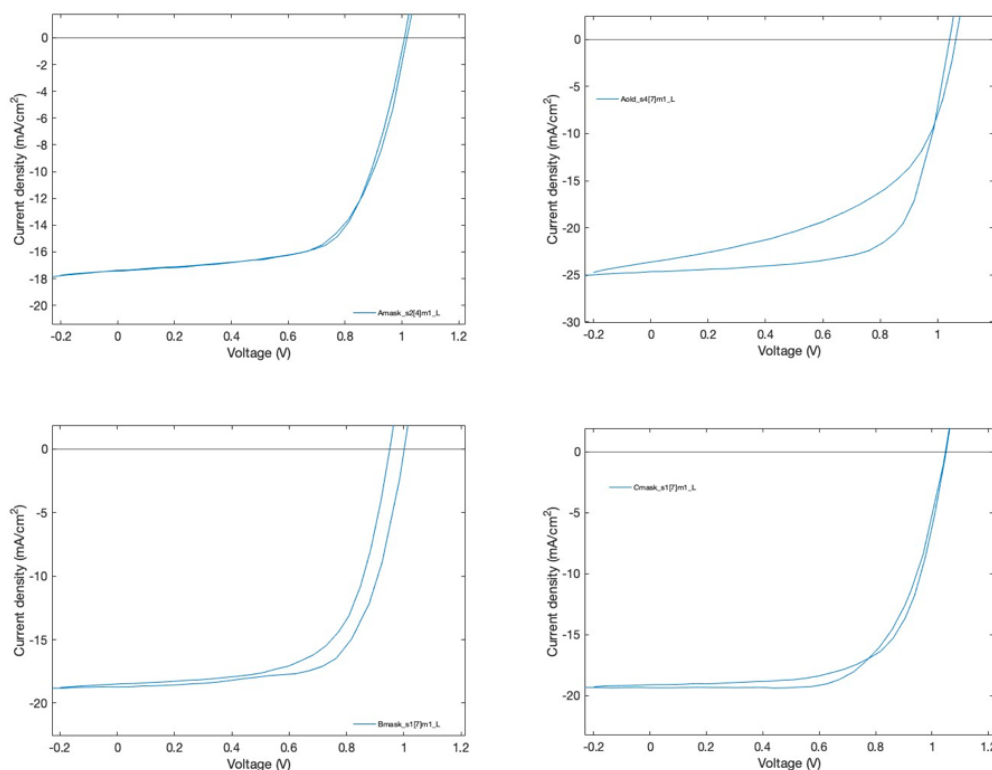


**Figure 4.5.** From left to right and up to down a) New  $\text{SnO}_2$  2.67 % b) 1-week-old  $\text{SnO}_2$  2.67 % c)  $\text{SnO}_2$  7.5 % d)  $\text{TiO}_2$ .

has also shown negligible hysteresis in previous studies.<sup>[2]</sup>

Moreover, external quantum efficiency (EQE) values of ETM  $\text{SnO}_2$  2.67 %,  $\text{SnO}_2$  7.5 % and  $\text{TiO}_2$  samples were also studied (Figure 4.6). ETM  $\text{SnO}_2$  2.67 % can reach EQE of 78 %, while ETM  $\text{SnO}_2$  7.5 % can reach EQE of 80 %. The shape and value of EQE graphs are quite similar to EQE results of  $\text{SnO}_2$ -based PSCs studies.<sup>[42]</sup> On the other hand, ETM  $\text{TiO}_2$  has shown higher EQE values, reaching almost 90 % efficiency. Therefore,  $\text{TiO}_2$ -based PSCs have higher EQE values than  $\text{SnO}_2$ -based PSCs, but their difference is not enormous.

The effect of different types of substrate (FTO and ITO) on the efficiency of  $\text{SnO}_2$ -based solar cells was also studied. From Table 4.3 and Figure 4.7 it can be seen that FTO  $\text{SnO}_2$  2.67 % resulted in both a higher PCE average value and the best PCE value. Both substrates had FF values of over 50 %. On the other hand, ITO-based samples showed less variation in PCE values. However, there might be other factors other than intrinsic factors of substrates that could affect the result. ITO substrates are significantly thinner than FTO substrates, which makes manufacturing steps such as spin-coating more challenging. There might be a higher chance of failing an ITO sample than an FTO sample. In addition, the number of FTO-based PSCs is more than ITO-based PSCs, which could also influence the results.

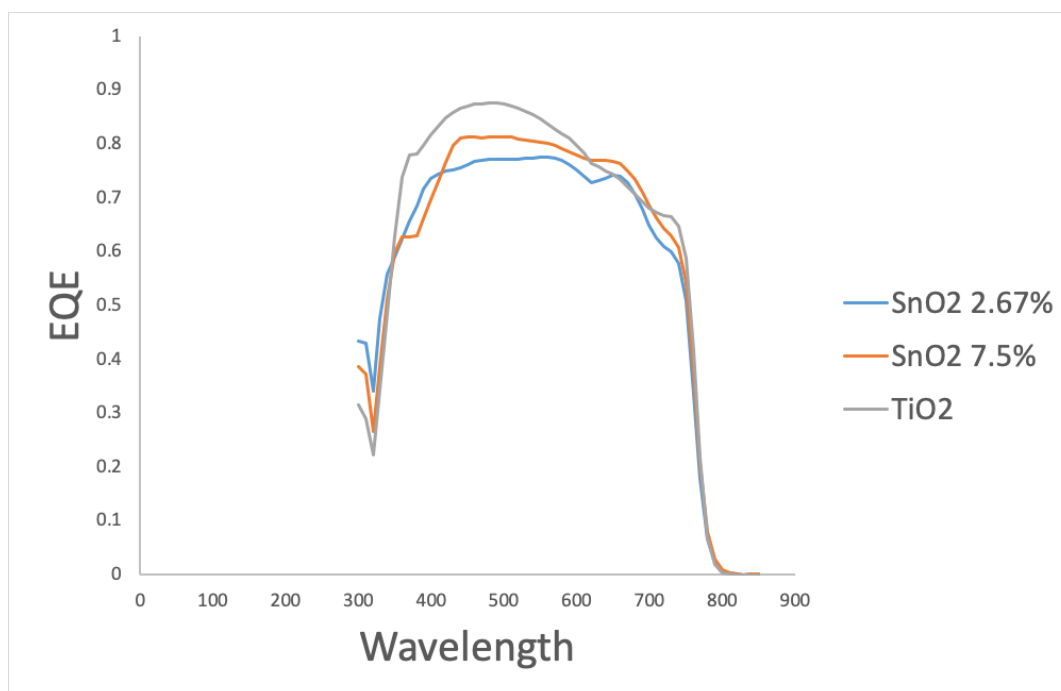


**Figure 4.6.** EQE results of FTO SnO<sub>2</sub> 2.67 %, FTO SnO<sub>2</sub> 7.5 % and FTO TiO<sub>2</sub>.

| Recipe | PCE (%)          | FF (%)           | $J_{sc}$ (mA/cm <sup>2</sup> ) | $V_{oc}$ (V)   | n   |
|--------|------------------|------------------|--------------------------------|----------------|-----|
| FTO    | 10.99<br>(15.67) | 54.67<br>(69.99) | 13.89<br>(23.68)               | 0.94<br>(1.07) | 136 |
| ITO    | 9.48<br>(14.40)  | 51.49<br>(65.11) | 18.90<br>(23.65)               | 0.85<br>(1.01) | 40  |

**Table 4.3.** Average and the best values of parameters for ETM SnO<sub>2</sub> 2.67 %, SnO<sub>2</sub> 7.5 %, TiO<sub>2</sub>. The best values are placed in brackets.

Hysteresis of FTO SnO<sub>2</sub> 2.67 % and ITO SnO<sub>2</sub> 2.67 % can be observed from Figure 4.8. FTO SnO<sub>2</sub> 2.67 % achieved noticeably less hysteresis than ITO SnO<sub>2</sub> 2.67 %, which resulted in a small gap between curves of reverse and forward sweep.

The improvement in PCE after some time of FTO SnO<sub>2</sub> 2.67 % and ITO 2.67 SnO<sub>2</sub> % was also studied. It can be seen from Figure 4.9 that both ITO and FTO-based SnO<sub>2</sub> 2.67 % cells resulted in improved PCE after 1 week. While FTO-based samples achieved higher PCE and also observed better improvement, ITO-based samples appeared to be more steady over a week and had less variation within the range of PCE.

In summary, SnO<sub>2</sub>-based solar cells resulted in promising PCE and other parameter values with small or negligible hysteresis. TiO<sub>2</sub>-based solar cell reached the highest PCE and EQE values compared to SnO<sub>2</sub>-based solar cell. However, over a period of time, SnO<sub>2</sub>-based solar cells have shown improvement in PCE more noticeably than TiO<sub>2</sub>-based solar cells. In addition, different SnO<sub>2</sub> concentrations might affect the performance

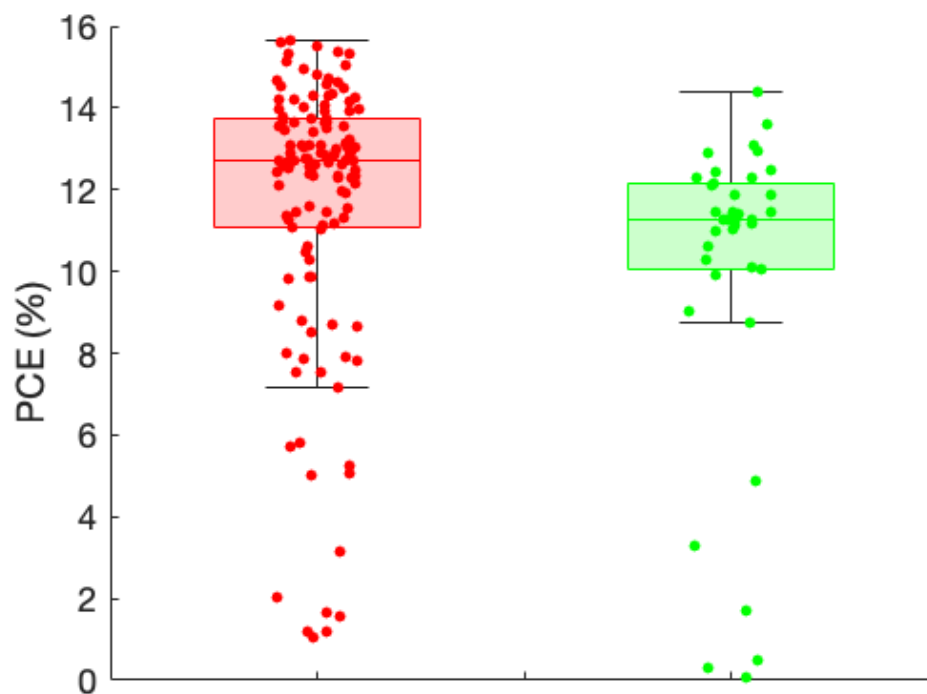


**Figure 4.7.** Boxplots of PCE values of FTO SnO<sub>2</sub> 2.67 % (left) and ITO SnO<sub>2</sub> 2.67 % (right).

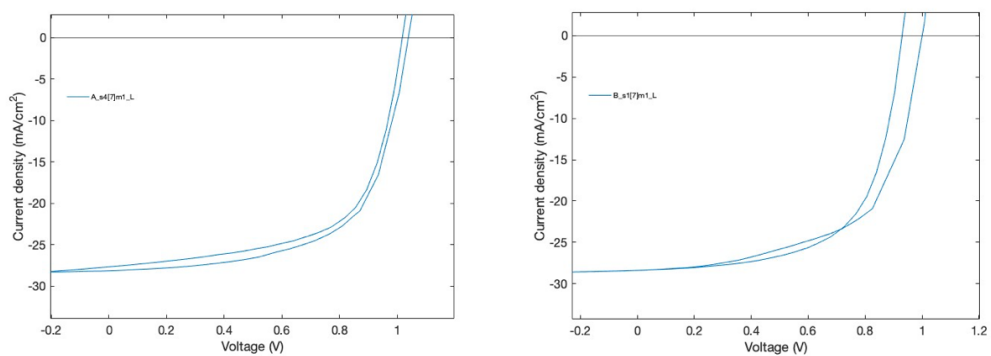


**Figure 4.8.** J-V curves of FTO and ITO SnO<sub>2</sub> 2.67 %

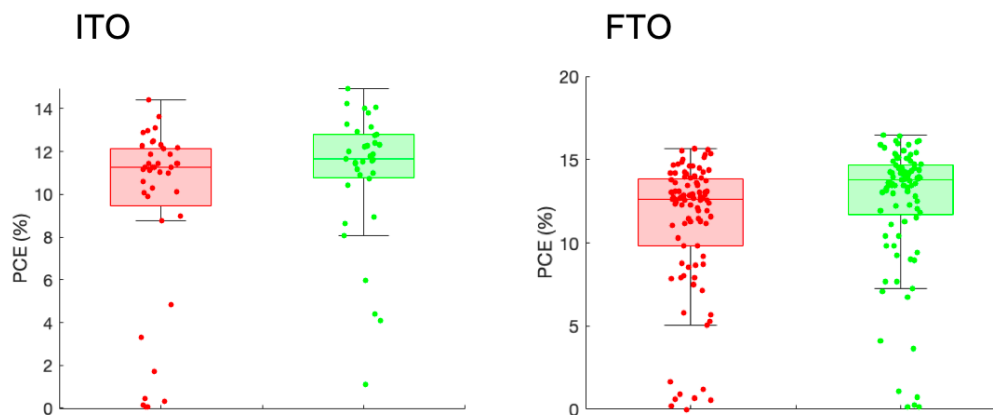


**Figure 4.9.** Power conversion efficiency (PCE) ITO (left) and FTO (right)  $\text{SnO}_2$  2.67 % after fabrication (red) and after 1 week (green).

of PSCs. In this study,  $\text{SnO}_2$  2.67 % PSCs had a more steady trend and less-varied PCE values than  $\text{SnO}_2$  7.5 % PSCs, even though  $\text{SnO}_2$  7.5 % PSCs might have shown more interpretable improvement in PCE over some time. FTO  $\text{SnO}_2$  2.67 % also achieved negligible hysteresis compared to FTO  $\text{SnO}_2$  7.5 % and FTO  $\text{TiO}_2$ . One interesting thing that could be studied further is the effect of time gap between the day of making ETM  $\text{SnO}_2$  solution and the day of using it in spincoating step on the performance of perovskite solar cell. 1-week-old  $\text{SnO}_2$  2.67 % sample has achieved higher PCE than freshly-made  $\text{SnO}_2$  2.67 % sample, even though the hysteresis of the former was noticeably bigger than the latter. Last but not least, FTO substrate achieved higher PCE in  $\text{SnO}_2$  2.67 % PSC than ITO substrate. Nevertheless, ITO-based samples have shown less variation within PCE range of values and might be more steady over time than FTO-based samples. Additionally, FTO substrate resulted in less hysteresis so it might be more suitable for  $\text{SnO}_2$ -based PSCs than ITO substrate.

## 4.2 Solar cell stability in MPPT measurement

The best-performing devices of both  $\text{TiO}_2$ -based perovskite solar cells and  $\text{SnO}_2$ -based perovskite solar cells were monitored with MPPT. The results of MPPT measurement of devices can be seen in Figure 4.10. The measurement was conducted over 100 hours in an inert atmosphere and no humidity to examine how PCE would drop over time and to compare stability between  $\text{TiO}_2$ -based solar cell and  $\text{SnO}_2$ -based solar cell.  $\text{TiO}_2$ -based solar cell performance appeared to be more stable and steady than  $\text{SnO}_2$ -based solar cell over a period of time. Its normalized PCE dropped to approximately 80 % and retained this value for several hours.

Between 0 and 10 hours, all samples had a drop of normalized PCE.  $\text{SnO}_2$ -based PSCs

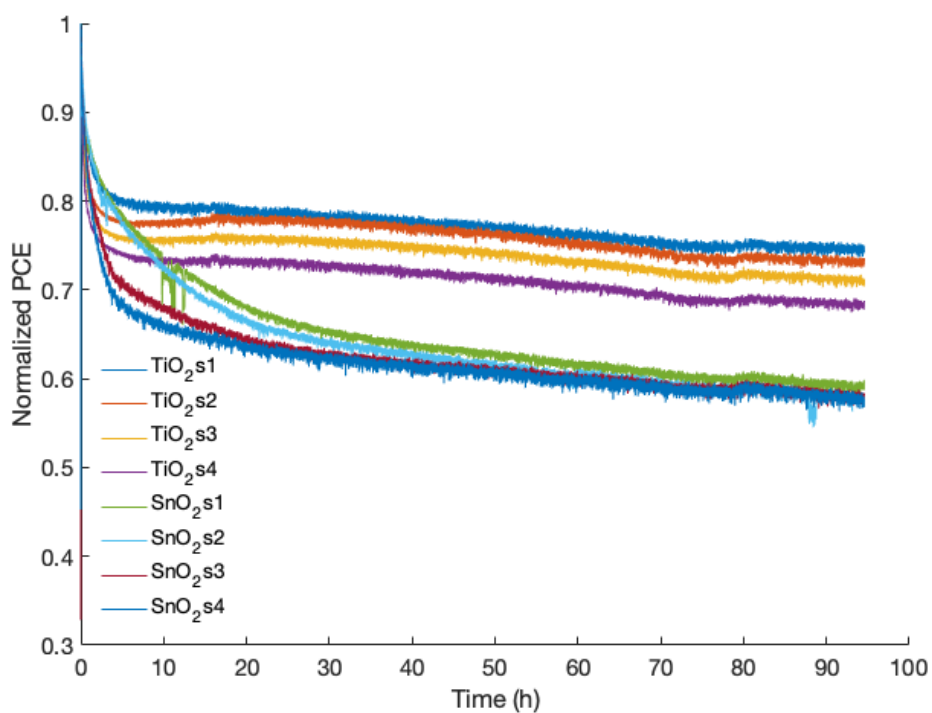


**Figure 4.10.** MPPT measurement results of 4 TiO<sub>2</sub>-based perovskite solar cells and 4 SnO<sub>2</sub>-based perovskite solar cells.

observed a bigger drop than TiO<sub>2</sub>-based PSCs did. Despite not having as impressive stability as TiO<sub>2</sub>-based solar cell, SnO<sub>2</sub>-based solar cell showed normalized PCE of approximately 60 % and noticeable steadiness over 100 hours. Therefore, SnO<sub>2</sub>-based perovskite solar cell can be considered as a highly stable device.

## 5. CONCLUSION

In this thesis, the effect of SnO<sub>2</sub> nanoparticles electron transport material (ETM) on lead-halide perovskite solar cell performance and stability was studied. The studied device structure was glass/planar SnO<sub>2</sub>/CsMAFA/spiro-OMETAD/Au. The used spiro-OMETAD hole transport material (HTM) was doped with tBP, Li-TFSI and FK209. The compact titanium dioxide (c-TiO<sub>2</sub>) combined with mesoporous titanium dioxide (m-TiO<sub>2</sub>) ETM was chosen as a reference. The reference device structure was glass/c-TiO<sub>2</sub>/m-TiO<sub>2</sub>/CsMAFA/spiro-OMETAD/Au.

First, when nanoparticle SnO<sub>2</sub> stock solution concentration was tested, the samples with SnO<sub>2</sub> 2.67 % assuming the stock concentration of 15 % achieved the best performance. The TiO<sub>2</sub>-based perovskite solar cell performed better than SnO<sub>2</sub>-based perovskite solar cell. The highest power conversion efficiency PCE reached by FTO TiO<sub>2</sub> was 17.88 % and the average PCE was 13.25 %. Its fill factor reached the highest value of 67.58 % and average value of 56.76 %. On the other hand, FTO SnO<sub>2</sub> 2.67 % reached the highest PCE of 14.60 % and average PCE of 11.3 %. The highest FF of FTO SnO<sub>2</sub> 2.67 % was 70.38 % and its average FF was 56.77 %. Even though the highest PCE reached by FTO SnO<sub>2</sub> 2.67 % was not as high as FTO TiO<sub>2</sub>, the gap between their average PCE values was not tremendous. PCE values of FTO SnO<sub>2</sub> 2.67 % samples were less varied than those of FTO TiO<sub>2</sub> samples. EQE value of TiO<sub>2</sub>-based PSCs was around 90 %, while EQE value of SnO<sub>2</sub> 2.67 % PSCs was around 80 %.

In addition, the highest PCE reached by FTO SnO<sub>2</sub> 7.5 % was higher than FTO SnO<sub>2</sub> 2.67 %. However, the average PCE and FF values of them were not noticeably different from each other. FTO and ITO were also compared to see which one can perform better with ETM SnO<sub>2</sub> in perovskite solar cell. FTO reached higher PCE and FF values than ITO, but ITO resulted in more steady SnO<sub>2</sub>-based PSCs.

Normalized PCE of TiO<sub>2</sub>-based solar cell was approximately 80 % of the initial recorded PCE for almost 100 hours. SnO<sub>2</sub>-based solar cell has shown that it can maintain approximately 60 % of the initial PCE over 100 hours.

In conclusion, although nanoparticle SnO<sub>2</sub>-based perovskite solar cell might not achieve parameters as high as TiO<sub>2</sub>-based PSC, it still yields promising results and has great potential. There is not an enormous gap between performance of TiO<sub>2</sub>-based PSC and

SnO<sub>2</sub>-based PSC. The manufacturing process of SnO<sub>2</sub>-based PSC does not require high-temperature step, which could remove the production cost and make the fabrication easier. Further research could study more SnO<sub>2</sub> recipes in PSC to improve the performance and stability of the device.

## REFERENCES

- [1] Yolcan, O. O. World energy outlook and state of renewable energy: 10-Year evaluation. *Innovation and Green Development* 2.4 (2023), p. 100070. ISSN: 2949-7531. DOI: <https://doi.org/10.1016/j.igd.2023.100070> URL: <https://www.sciencedirect.com/science/article/pii/S2949753123000383>.
- [2] Zheng, J. and Zeng, B. Unleashing the influencing factors of solar energy adoption to combat climate change: A roadmap toward sustainable energy technologies. *Sustainable Energy Technologies and Assessments* 57 (2023), p. 103303. ISSN: 2213-1388. DOI: <https://doi.org/10.1016/j.seta.2023.103303> URL: <https://www.sciencedirect.com/science/article/pii/S2213138823002965>
- [3] Wang, Q., Yang, T. and Li, R. Does income inequality reshape the environmental Kuznets curve (EKC) hypothesis? A nonlinear panel data analysis. *Environmental Research* 216 (2023), p. 114575. ISSN: 0013-9351. DOI: <https://doi.org/10.1016/j.envres.2022.114575> URL: <https://www.sciencedirect.com/science/article/pii/S0013935122019028>.
- [4] Ekener-Petersen, E., Höglund, J. and Finnveden, G. Screening potential social impacts of fossil fuels and biofuels for vehicles. *Energy Policy* 73 (2014), pp. 416–426. ISSN: 0301-4215. DOI: <https://doi.org/10.1016/j.enpol.2014.05.034> URL: <https://www.sciencedirect.com/science/article/pii/S0301421514003334>
- [5] Fraser, T., Chapman, A. J. and Shigetomi, Y. Leapfrogging or lagging? Drivers of social equity from renewable energy transitions globally. *Energy Research & Social Science* 98 (2023), p. 103006. ISSN: 2214-6296. DOI: <https://doi.org/10.1016/j.erss.2023.103006> URL: <https://www.sciencedirect.com/science/article/pii/S221462962300066X>.
- [6] Ahmad, F., Draz, M. U., Chandio, A. A., Ahmad, M., Su, L., Shahzad, F. and Jia, M. Natural resources and environmental quality: Exploring the regional variations among Chinese provinces with a novel approach. *Resources Policy* 77 (2022), p. 102745. ISSN: 0301-4207. DOI: <https://doi.org/10.1016/j.resourpol.2022.102745> URL: <https://www.sciencedirect.com/science/article/pii/S0301420722001933>
- [7] Hasnain, S. M. Examining the advances, obstacles, and achievements of tin-based perovskite solar cells: a review. *Solar Energy* 262 (2023), p. 111825. ISSN: 0038-092X. DOI: <https://doi.org/10.1016/j.solener.2023.111825> URL: <https://www.sciencedirect.com/science/article/pii/S0038092X23004504>

- [8] Ren, Y., Liu, X., Li, H., Qin, J., Du, S., Lu, X., Tong, J., Yang, C. and Li, J. Utilizing non-conjugated small-molecular tetrasodium iminodisuccinate as electron transport layer enabled improving efficiency of organic solar cells. *Optical Materials* 129 (2022), p. 112520. ISSN: 0925-3467. DOI: <https://doi.org/10.1016/j.optmat.2022.112520> URL: <https://www.sciencedirect.com/science/article/pii/S0925346722005547>
- [9] Chowdhury, T. A., Bin Zafar, M. A., Sajjad-Ul Islam, M., Shahinuzzaman, M., Islam, M. A. and Khandaker, M. U. Stability of perovskite solar cells: issues and prospects. *RSC Adv.* 13 (3 2023), pp. 1787–1810. DOI: [10.1039/D2RA05903G](https://doi.org/10.1039/D2RA05903G) URL: <http://dx.doi.org/10.1039/D2RA05903G>
- [10] Mellit, A. and Kalogirou, S. 1 - Solar radiation and photovoltaic systems: Modeling and simulation. *Handbook of Artificial Intelligence Techniques in Photovoltaic Systems*. Ed. by A. Mellit and S. Kalogirou. Academic Press, 2022, pp. 1–41. ISBN: 978-0-12-820641-6. DOI: <https://doi.org/10.1016/B978-0-12-820641-6.00001-6> URL: <https://www.sciencedirect.com/science/article/pii/B9780128206416000016>
- [11] Shur, M. *Physics of Semiconductor Devices*. Prentice-Hall series in solid state physical electronics. Prentice Hall, 1990. ISBN: 9780136664963. URL: <https://books.google.fi/books?id=io40nwEACAAJ>
- [12] Häberlin, H. *Photovoltaics: System Design and Practice*. Wiley, 2012. ISBN: 9781119978381. URL: <https://books.google.fi/books?id=w8k3aXBnDP4C>
- [13] Woodhouse, M., Jones-Albertus, R., Feldman, D., Fu, R., Horowitz, K., Chung, D., Jordan, D. and Kurtz, S. On the Path to SunShot. The Role of Advancements in Solar Photovoltaic Efficiency, Reliability, and Costs. (May 2016). DOI: [10.2172/1253983](https://doi.org/10.2172/1253983) URL: <https://www.osti.gov/biblio/1253983>
- [14] Würfel, U., Cuevas, A. and Wuerfel, P. Charge Carrier Separation in Solar Cells. *Photovoltaics, IEEE Journal of PP* (Jan. 2014), pp. 1–9. DOI: [10.1109/JPHOTOV.2014.2363550](https://doi.org/10.1109/JPHOTOV.2014.2363550)
- [15] Hubbard, S. Recombination. *Photovoltaic Solar Energy*. John Wiley & Sons, Ltd, 2016. Chap. 2.4, pp. 39–46. ISBN: 9781118927496. DOI: <https://doi.org/10.1002/9781118927496.ch5> URL: <https://onlinelibrary.wiley.com/doi/abs/10.1002/9781118927496.ch5>
- [16] Smets, A., Jäger, K., Isabella, O., van Swaaij, R. and Zeman, M. *Solar Energy: The physics and engineering of photovoltaic conversion, technologies and systems*. English. UIT Cambridge Limited, 2016. ISBN: 978-1-906860-32-5.
- [17] Zhao, D., Yu, Y., Wang, C., Liao, W., Shrestha, N., Grice, C., Cimaroli, A., Guan, L., Ellingson, R., Zhu, K., Zhao, X., Xiong, R.-G. and Yan, Y. Low-bandgap mixed tin–lead iodide perovskite absorbers with long carrier lifetimes for all-perovskite tandem solar cells. *Nature Energy* 2 (Mar. 2017), p. 17018. DOI: [10.1038/nenergy.2017.18](https://doi.org/10.1038/nenergy.2017.18)

- [18] Kamran, M. Chapter 5 - Planning and modeling of solar energy systems. Dec. 2022, pp. 219–270. ISBN: 978-0-323-99560-3. DOI: [10.1016/B978-0-323-99560-3.00004-1](https://doi.org/10.1016/B978-0-323-99560-3.00004-1)
- [19] Cheng, Y. and Ding, L. Pushing commercialization of perovskite solar cells by improving their intrinsic stability. *Energy Environ. Sci.* 14 (6 2021), pp. 3233–3255. DOI: [10.1039/D1EE00493J](https://doi.org/10.1039/D1EE00493J) URL: <http://dx.doi.org/10.1039/D1EE00493J>
- [20] Roy, P., Sinha, N., Tiwari, S. and Khare, A. A review on perovskite solar cells: Evolution of architecture, fabrication techniques, commercialization issues and status. *Solar Energy* 198 (Mar. 2020), pp. 665–688. DOI: [10.1016/j.solener.2020.01.080](https://doi.org/10.1016/j.solener.2020.01.080)
- [21] Zhao, X. and Park, N.-G. Stability Issues on Perovskite Solar Cells. *Photonics* 2 (Nov. 2015), pp. 1139–1151. DOI: [10.3390/photonics2041139](https://doi.org/10.3390/photonics2041139)
- [22] Badia, L., Mas-Marzá, E., Sánchez Sánchez, R., Barea, E., Bisquert, J. and Mora-Seró, I. New iridium complex as additive to the spiro-OMeTAD in perovskite solar cells with enhanced stability. *APL Materials* 2 (Aug. 2014), p. 081507. DOI: [10.1063/1.4890545](https://doi.org/10.1063/1.4890545)
- [23] Waththage, S. C., Song, Z., Phillips, A. B. and Heben, M. J. Chapter 3 - Evolution of Perovskite Solar Cells. *Perovskite Photovoltaics*. Ed. by S. Thomas and A. Thankappan. Academic Press, 2018, pp. 43–88. ISBN: 978-0-12-812915-9. DOI: <https://doi.org/10.1016/B978-0-12-812915-9.00003-4> URL: <https://www.sciencedirect.com/science/article/pii/B9780128129159000034>
- [24] Green, M., Ho-Baillie, A. and Snaith, H. The emergence of perovskite solar cells. *Nature Photonics* 8 (July 2014). DOI: [10.1038/NPHOTON.2014.134](https://doi.org/10.1038/NPHOTON.2014.134)
- [25] Kojima, A., Teshima, K., Miyasaka, T. and Shirai, Y. Novel Photoelectrochemical Cell with Mesoscopic Electrodes Sensitized by Lead-Halide Compounds (2). 2006. URL: <https://api.semanticscholar.org/CorpusID:137886120>
- [26] Kojima, A., Teshima, K., Shirai, Y. and Miyasaka, T. Organometal Halide Perovskites as Visible-Light Sensitizers for Photovoltaic Cells. *Journal of the American Chemical Society* 131 (May 2009), pp. 6050–1. DOI: [10.1021/ja809598r](https://doi.org/10.1021/ja809598r)
- [27] Im, J.-H., Lee, C.-R., Lee, J.-W., Park, S.-W. and Park, N.-G. 6.5 % efficient perovskite quantum-dot-sensitized solar cell. *Nanoscale* 3 (Sept. 2011), pp. 4088–93. DOI: [10.1039/c1nr10867k](https://doi.org/10.1039/c1nr10867k)
- [28] Lee, M., Teuscher, J., Miyasaka, T., Murakami, T. and Im, J.-H. Efficient Hybrid Solar Cells Based on Meso-Superstructured Organometal Halide Perovskites. *Science (New York, N.Y.)* 338 (Oct. 2012). DOI: [10.1126/science.1228604](https://doi.org/10.1126/science.1228604)
- [29] (NREL), N. R. E. L. *Best Research-Cell Efficiency Chart*. Accessed on 17/08/2023. 2023. URL: <https://www.nrel.gov/pv/cell-efficiency.html>
- [30] Rajagopal, A., Yao, K. and Jen, A. Toward Perovskite Solar Cell Commercialization: A Perspective and Research Roadmap Based on Interfacial Engineering. *Advanced Materials* 30 (June 2018). DOI: [10.1002/adma.201800455](https://doi.org/10.1002/adma.201800455)

- [31] Werner, J., Weng, C.-H., Walter, A., Fesquet, L., Seif, J., De Wolf, S., Niesen, B. and Ballif, C. Efficient Monolithic Perovskite/Silicon Tandem Solar Cell With Cell Area > 1 cm<sup>2</sup>. *Journal of Physical Chemistry Letters* 7 (Dec. 2015), pp. 161–166. DOI: [10.1021/acs.jpcllett.5b02686](https://doi.org/10.1021/acs.jpcllett.5b02686).
- [32] Albrecht, S., Saliba, M., Correa-Baena, J.-P., Lang, F., Kegelman, L., Mews, M., Steier, L., Abate, A., Rappich, J., Korte, L., Schlattmann, R., Nazeeruddin, M., Hagfeldt, A., Grätzel, M. and Rech, B. Monolithic Perovskite/Silicon-Heterojunction Tandem Solar Cells Processed at Low Temperature. *Energy & Environmental Science* (Nov. 2015), p. 8188. DOI: [10.1039/C5EE02965A](https://doi.org/10.1039/C5EE02965A).
- [33] De Wolf, S. and Aydin, E. Tandems have the power. *Science (New York, N.Y.)* 381 (July 2023), pp. 30–31. DOI: [10.1126/science.adi6278](https://doi.org/10.1126/science.adi6278).
- [34] Boyd, C., Cheacharoen, R., Leijtens, T. and McGehee, M. Understanding Degradation Mechanisms and Improving Stability of Perovskite Photovoltaics. *Chemical Reviews* 119 (Nov. 2018). DOI: [10.1021/acs.chemrev.8b00336](https://doi.org/10.1021/acs.chemrev.8b00336).
- [35] Manjunath, V., Krishna, R., Maniarasu, S., Ramasamy, E., Shanmugasundaram, S. and Veerappan, G. Chapter 4 - Perovskite Solar Cell Architectures. *Perovskite Photovoltaics*. Ed. by S. Thomas and A. Thankappan. Academic Press, 2018, pp. 89–121. ISBN: 978-0-12-812915-9. DOI: <https://doi.org/10.1016/B978-0-12-812915-9.00004-6>. URL: <https://www.sciencedirect.com/science/article/pii/B9780128129159000046>.
- [36] Pradid, P., Sanglee, K., Thongprong, N. and Chuangchote, S. Carbon Electrodes in Perovskite Photovoltaics. *Materials* 14 (Oct. 2021), p. 5989. DOI: [10.3390/ma14205989](https://doi.org/10.3390/ma14205989).
- [37] Jiang, Q., Zhang, L. Q., Wang, H., Yang, X., Meng, J., Liu, H., Yin, Z., Wu, J., Zhang, X. and You, J. Enhanced electron extraction using SnO<sub>2</sub> for high-efficiency planar-structure HC(NH<sub>2</sub>)<sub>2</sub>PbI<sub>3</sub>-based perovskite solar cells. *Nature Energy* 2 (2016). URL: <https://api.semanticscholar.org/CorpusID:100003370>.
- [38] Seo, J.-Y., Matsui, T., Luo, J., Correa-Baena, J.-P., Giordano, F., Saliba, M., Schenk, K., Ummadisingu, A., Domanski, K., Hadadian, M., Hagfeldt, A., Zakeeruddin, S. M., Steiner, U., Grätzel, M. and Abate, A. Ionic Liquid Control Crystal Growth to Enhance Planar Perovskite Solar Cells Efficiency. *Advanced Energy Materials* 6.20 (2016), p. 1600767. DOI: <https://doi.org/10.1002/aenm.201600767> eprint: <https://onlinelibrary.wiley.com/doi/pdf/10.1002/aenm.201600767>. URL: <https://onlinelibrary.wiley.com/doi/abs/10.1002/aenm.201600767>.
- [39] Mahmood, K., Sarwar, S. and Mehran, T. Current status of electron transport layers in perovskite solar cells: materials and properties. *RSC Adv.* 7 (Mar. 2017), pp. 17044–17062. DOI: [10.1039/C7RA00002B](https://doi.org/10.1039/C7RA00002B).
- [40] Lee, Y., Paek, S., Cho, K., Oveisi, E., Gao, P., Lee, S.-H., Park, J.-S., Zhang, y., Humphry-Baker, R., Asiri, A. M. and Nazeeruddin, M. Enhanced Charge Collection

- with Passivation of the Tin Oxide Layer in Planar Perovskite Solar Cells. *J. Mater. Chem. A* 5 (June 2017). DOI: [10.1039/C7TA04128D](https://doi.org/10.1039/C7TA04128D).
- [41] anaraki, E. halvani, Kermanpur, A., Steier, L., Domanski, K., Matsui, T., Tress, W., Saliba, M., Abate, A., Graetzel, M., Hagfeldt, A. and Correa-Baena, J.-P. Highly efficient and stable planar perovskite solar cells by solution-processed tin oxide. *Energy Environ. Sci.* 9 (Sept. 2016). DOI: [10.1039/C6EE02390H](https://doi.org/10.1039/C6EE02390H).
- [42] Zhang, K., Duan, J., Liu, F., Zhang, J. and Wang, H. Low-temperature-deposited SnO<sub>2</sub> films for efficient planar CH<sub>3</sub>NH<sub>3</sub>PbI<sub>3</sub> photovoltaics. *Journal of Materials Science* 56 (Jan. 2021), pp. 1–14. DOI: [10.1007/s10853-020-05216-y](https://doi.org/10.1007/s10853-020-05216-y)
- [43] Wang, Z., Fang, J., Mi, Y., Zhu, X., Ren, H., Liu, X. and Yan, Y. Enhanced Performance of Perovskite Solar Cells by Ultraviolet-Ozone Treatment of Mesoporous TiO<sub>2</sub>. *Applied Surface Science* 436 (Dec. 2017). DOI: [10.1016/j.apsusc.2017.12.085](https://doi.org/10.1016/j.apsusc.2017.12.085).
- [44] Khaleda, F., Balakrishnan, V. and Abd Rahim, N. Spectral response and quantum efficiency evaluation of solar cells: a review. Jan. 2021, pp. 525–566. ISBN: 9780128237106. DOI: [10.1016/B978-0-12-823710-6.00014-5](https://doi.org/10.1016/B978-0-12-823710-6.00014-5)
- [45] Mahato, G., Biswal, S., Roy Choudhury, T., Nayak, B. and Santra, S. Review of active power control techniques considering the impact of MPPT and FPPT during high PV penetration. *Solar Energy* 251 (Feb. 2023), pp. 404–419. DOI: [10.1016/j.solener.2023.01.035](https://doi.org/10.1016/j.solener.2023.01.035)
- [46] Khenkin, M., Katz, E., Abate, A., Bardizza, G., Berry, J., Brabec, C., Brunetti, F., Bulovic, V., Burlingame, Q., Di Carlo, A., Cheacharoen, R., Bing, C., Colsmann, A., Cros, S., Domanski, K., Dusza, M., Fell, C., Forrest, S., Galagan, Y. and Lira-Cantu, M. Consensus statement for stability assessment and reporting for perovskite photovoltaics based on ISOS procedures. *Nature Energy* 5 (Jan. 2020), pp. 35–49. DOI: [10.1038/s41560-019-0529-5](https://doi.org/10.1038/s41560-019-0529-5).